JGR Oceans

RESEARCH ARTICLE
10.1029/2018JC014700

A Comparison of the Atlantic and Pacific Bjerknes Feedbacks: Seasonality, Symmetry, and Stationarity

T. Dippe[1], **J. F. Lübbecke**[1,2], **and R. J. Greatbatch**[1,2]

[1]GEOMAR Helmholtz Centre for Ocean Research Kiel, Kiel, Germany, [2]Faculty of Mathematics and Natural Sciences, Christian Albrechts University, Kiel, Germany

Key Points:
- The elements of the Atlantic Bjerknes feedback display asymmetries
- These asymmetries are less consistent in the Atlantic, compared to their Pacific counterparts
- The Atlantic Bjerknes feedback varies substantially on decadal time scales

Correspondence to:
T. Dippe,
tdippe@geomar.de

Citation:
Dippe, T., Lübbecke, J. F., & Greatbatch, R. J. (2019). A comparison of the Atlantic and Pacific Bjerknes feedbacks: Seasonality, symmetry, and stationarity. *Journal of Geophysical Research: Oceans*, *124*, 2374–2403. https://doi.org/10.1029/2018JC014700

Received 19 OCT 2018
Accepted 13 MAR 2019
Accepted article online 18 MAR 2019
Published online 4 APR 2019

Abstract The Bjerknes feedback is the dominant positive feedback in the equatorial ocean basins. To examine the seasonality, symmetry, and stationarity of the Pacific and Atlantic Bjerknes feedbacks we decompose them into three feedback elements that relate thermocline depth, sea surface temperature, and western basin wind stress variability to each other. We partition feedback elements into composites associated with positive or negative anomalies. Using robust regression, we diagnose the strength of each composite. For the recent period 1993–2012, composites of the Pacific Bjerknes feedback elements agree well with previous work. Positive composites are generally stronger than negative composites, and all feedback elements are weakest in late boreal spring. In the Atlantic, differences between positive and negative composites are less consistent across feedback elements. Specifically, wind variability seems to play a less important role in shaping atmosphere-ocean coupling in the Atlantic when compared to the Pacific. However, a clear seasonality emerges: Feedback elements are generally strong in boreal summer and, for the negative composites, again in boreal winter. The Atlantic Bjerknes feedback is dominated by subsurface-surface coupling. Applying our analysis to overlapping 25-year periods for 1958–2009 shows that the strengths of feedback elements in both ocean basins vary on decadal time scales. While the overall asymmetry of the Pacific Bjerknes feedback is robust, the strength and symmetry of Atlantic feedback elements vary considerably between decades. Our results indicate that the Atlantic Bjerknes feedback is nonstationary on decadal time scales.

1. Introduction

The Bjerknes feedback is the dominant coupled, positive feedback in the equatorial oceans (Bjerknes, 1966, 1969). It plays a crucial role in shaping Atlantic and Pacific equatorial variability, tying three key properties of an equatorial ocean basin into a closed feedback loop. These properties are the thermocline depth along the equator, which can be approximated by sea surface height (SSH) in the central and eastern ocean basin (Cane, 1984; Rebert et al., 1985); eastern basin sea surface temperature (SST); and western basin zonal wind stress (USTR). The closed feedback loop operates as a positive feedback for both positive and negative anomalies in either SSH, SST, or USTR and can be decomposed into three feedback elements that act in concert:

(i) SSH→ SST: *Subsurface-surface coupling*. The thermocline depth in the eastern ocean basin is related to net upwelling of cold water into the surface mixed layer, and mixing at the base of the mixed layer (Hummels et al., 2013). Variations of thermocline depth are related to variations in the local warm water volume that in turn affects how effectively upwelling alters the mixed layer temperature.

(ii) SST→ USTR: *SST-wind coupling*. Eastern basin SST anomalies produce a local, Gill-type atmospheric response (Gill, 1980) that alters the sea level pressure gradient along the equator and affects surface winds in the western ocean basin.

(iii) USTR → SSH: *Wind-thermocline coupling*. Zonal wind anomalies in the western ocean basin change the local balance between zonal wind stress and the subsurface pressure gradient in the ocean. The thermocline adapts to the varying subsurface pressure gradient and transmits the information eastward along the equator via an equatorial Kelvin wave. In the eastern ocean basin, thermocline variability couples to SST variability and closes the Bjerknes feedback loop.

Since Bjerknes (1966) first described the closed feedback loop outlined above, different studies have referred to different mechanisms as "the Bjerknes feedback," sometimes focusing on the atmospheric or ocean parts of the coupled feedback only. Here, when we discuss "the" Bjerknes feedback, we refer to the coupled feedback that links oceanic and atmospheric variability.

In the equatorial Atlantic and Pacific Oceans, the Bjerknes feedback supports the growth of coupled air-sea anomalies associated with the Atlantic and Pacific Niños (Bjerknes, 1969; Burls et al., 2012; Deppenmeier et al., 2016; Dippe et al., 2018; Keenlyside & Latif, 2007; Lübbecke & McPhaden, 2013). While the phrase "Pacific Niño" in a strict sense refers to the SST manifestation of a positive El Niño–Southern Oscillation (ENSO) event, we use the name to refer to the entire coupled process. Likewise, when we talk about the "Atlantic Niño," we mean the complete coupled atmosphere-ocean process, including negative events that are generally known as Niñas.

In their respective basins, the Niños are the dominant mode of interannual SST variability. While their corresponding names and similar patterns suggest that they are essentially manifestations of the same process, significant differences exist (Burls et al., 2011; Keenlyside & Latif, 2007; Lübbecke & McPhaden, 2013; Richter et al., 2013; Xie et al., 1999). The canonical Pacific Niño generally peaks in boreal winter and lasts for several months, while the Atlantic Niño is tightly phase-locked to boreal summer and rarely outlasts a season, achieving roughly half of the Pacific SST anomaly amplitude. The phase locking of the Niños is accompanied by a strong seasonality of their supporting Bjerknes feedbacks. The Pacific Bjerknes feedback operates for most of the year, while the Atlantic Bjerknes feedback is active for a few months only twice a year, in boreal summer and again, briefly, at the beginning of boreal winter (Burls et al., 2011; Dippe et al., 2018).

Another interesting feature of the Atlantic is that it hosts a secondary, Niño-like phenomenon in boreal winter. Okumura and Xie (2006) found that the "winter Niño"—their "Niño II"—is the product of a secondary, seasonal weakening of the trade winds in the Gulf of Guinea, which is able to briefly organize coupled atmosphere-ocean variability into the Bjerknes feedback.

Characteristics of the Atlantic and Pacific Niños vary on decadal and longer time scales. Losada and Rodríguez-Fonseca (2016) and Martín-Rey et al. (2017) report that the Atlantic Multidecadal Oscillation (AMO)—a low-frequency phenomenon that is mainly characterized by variations of basin-wide SST in the North Atlantic (Delworth & Mann, 2000; Knight et al., 2006; Schlesinger & Ramankutty, 1994)—modulates both the spatial configuration of the Atlantic Niño SST pattern and the atmospheric response to these patterns. Martín-Rey et al. (2017) argue that eastern equatorial Atlantic SST variability is enhanced by more than 150% in boreal summer during negative AMO phases. Similarly, Cobb et al. (2013) and Li et al. (2013) demonstrate for centennial and millennial time scales that the spatiotemporal characteristics of the Pacific Niño are subject to low-frequency variations. For the recent decades, Lübbecke et al. (2014) show that low-frequency variations in the Pacific background state modulate the strength of the Pacific Bjerknes feedback and hence the characteristics of the Pacific Niño.

The spatiotemporal characteristics of warm and cold Pacific Niño events are subject to a number of asymmetries (Capotondi et al., 2015; Chen et al., 2015; Dommenget et al., 2013; Takahashi et al., 2011; Takahashi & Dewitte, 2016). Warm events are generally stronger in terms of their SST amplitude than cold events, while cold events last longer and evolve in a different spatial manner. Another aspect of the complex nature of the Pacific Niño is highlighted by the existence of different manifestations of Pacific Niño events that appear to have distinct spatiotemporal signatures (Capotondi et al., 2015; Takahashi et al., 2011; Takahashi & Dewitte, 2016; Yeh et al., 2009). Yeh et al. (2009) document that the last decades saw an increase in the frequency of the central Pacific Niño. In contrast to the canonical eastern Pacific Niño with its clear signature in the eastern Pacific and seesaw response in the anomalous Walker circulation, the pattern of the central Pacific Niño is constrained to the region between 160°E and 120°W and splits the Walker circulation into two cells (Ashok & Yamagata, 2009). A generalization of these ENSO "flavors" has recently been proposed by Timmermann et al. (2018), who provide an overview on what they call ENSO complexity.

Some of the above asymmetries in the Pacific have been linked to asymmetries in the strength of the Pacific Bjerknes feedback elements. Dommenget et al. (2013) and DiNezio and Deser (2014) show that the different lengths of warm and cold events are related to nonlinearities in the SSH-SST and SST-USTR feedback elements. In a different approach, Hu et al. (2017) shows that the "recharge/discharge" processes associated

with wind-thermocline coupling operate differently for warm and cold events, favoring long cold events and rather short, intense warm events. Levine and McPhaden (2016) show that state-dependent noise forcing contributes to the SST amplitude asymmetry of the Pacific Niño. State-dependent noise provides an additional positive feedback between warm Pacific Niño events and zonal wind variability. The evolving warm event amplifies its own wind forcing by creating a state that promotes the occurrence of subsequent strong westerly wind bursts in the western and central ocean basin. This mechanism enhances wind-thermocline coupling.

In contrast to the prominent Pacific SST amplitude asymmetry, the Atlantic Niño is rather symmetric. Lübbecke and McPhaden (2017) show that warm and cold Atlantic Niño events are effectively mirror images of each other. Additionally, they diagnose the strength of the Bjerknes feedback elements for both positive and negative summer events and conclude that, unlike the Pacific Bjerknes feedback, the Atlantic summer Bjerknes feedback is largely symmetric.

Here, we revisit the work of Lübbecke and McPhaden (2017) by taking into account zonal, seasonal, and decadal variations of the Bjerknes feedback strengths associated with positive and negative events in the equatorial Atlantic. Specifically, we seek to answer the following question: For the summer and winter Niños in the equatorial Atlantic, does the Bjerknes feedback operate symmetrically for cold and warm events? Are these findings stationary, or do they depend on the analysis period?

The remainder of this study is structured as follows. Section 2 explains how we estimate the Bjerknes feedback and on which data sets we base our analysis. Section 3 discusses the results of our analysis. In section 4, we compare our findings with the work of Lübbecke and McPhaden (2017) and attempt to assess the stationarity of our results. A discussion is provided in the last section.

2. Data and Methods

2.1. Data

Our analysis is based on two groups of data sets that each contain monthly mean SSH, SST, and USTR in the equatorial Atlantic and Pacific ocean basins.

1. *OBS*, 1993–2012, direct satellite observations, reconstructions, and reanalysis. We use SSH provided by AVISO (`https://www.aviso.altimetry.fr/en/home.html`); SST from NOAA's Extended Reconstructed Sea Surface Temperature (Smith & Reynolds, 2003, ERSST), version 5 (Huang et al., 2017); and USTR from the ERA-Interim Reanalysis (Dee et al., 2011). While ERA-Interim is not an observational data set, we call this group "OBS" for the sake of readability.
2. *ORAS4*, 1958–2009, ECMWF's Ocean Reanalysis System Version 4 (Balmaseda et al., 2012), which provides dynamically consistent SSH, SST, and USTR. SSH and three-dimensional ocean potential temperature data were downloaded from the University of Hamburg's Integrated Climate Data Center (`http://icdc.cen.uni-hamburg.de/projek-te/easy-init/-easy-init-ocean.html`). We use SSH as provided by the reanalysis; the first level of the ocean potential temperature as SST; and the same wind stress data set as in Lübbecke and McPhaden (2017). This corresponds to the wind stress forcing of ORAS4, using ERA-40 (Uppala et al., 2006) data from January 1958 to December 1988, and ERA-Interim data afterward. Note that reanalysis products potentially suffer from model-induced biases and that the accuracy of results is highly sensitive to the quality of the assimilated data. Uncertainties are generally larger prior to the advent of satellite observations in the late 1970s. Because of this, our discussion of ORAS4-based results in section 4 will focus on general issues rather than on exact numerical values.

As pointed out in section 1, SSH is a reliable proxy for thermocline depth in the central and eastern equatorial ocean basins only (Cane, 1984). Hence, results involving SSH should be treated cautiously in the western warm pool regions.

Anomalies in this study are calculated as follows: We first remove the linear trend from the entire time series, then subtract the seasonal cycle to obtain monthly anomalies. For each analysis, we calculate the anomalies with respect to the chosen analysis periods.

For the overlap period 1993–2009, we compare the time series of anomalies and the seasonal distribution of standard deviations between the two data set groups for each variable (Figure 1). To facilitate comparison, we average our data into indices of the Atl3 and Nino3.4 regions (3°S to 3°N, 20°W to 0°E, and 5°S to 5°N,

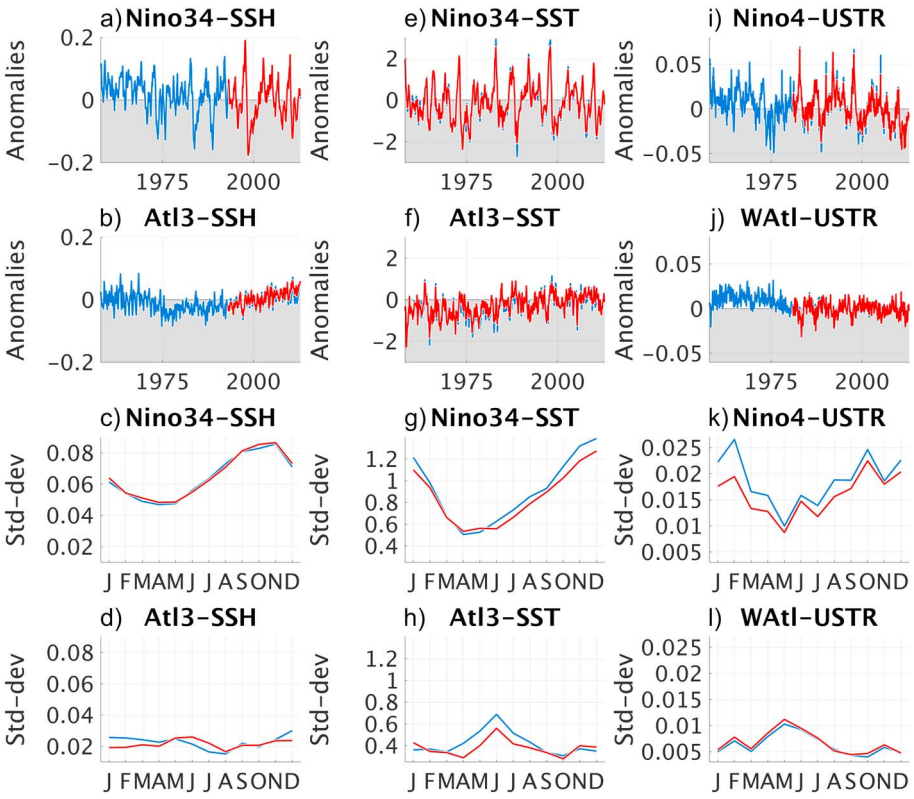

Figure 1. Key features of employed data sets. Time series of anomalies with respect to the linear trend and the seasonal cycle (upper two rows, panels a, b, e–f, i–j), and monthly stratified standard deviations (lower two rows, c, d, g, h, k, l, months from January to December indicated by their first letter on the *x* axis). Both quantities have been diagnosed with respect to the overlap period of the two data set groups, 1993–2009. Each panel shows the same quantity for the OBS and ORAS4 data set groups as red and blue lines, respectively, and all quantities are shown for SSH, SST, and USTR in the left column (a–d), middle column (e–h), and right column (i–l). The OBS group contains AVISO-SSH, ERSST-SST, and ERA-Interim zonal wind stress (USTR). Data have been averaged into the Atl3 and Nino3.4 regions in the Atlantic and Pacific for both SSH and SST; and into the WAtl and Nino4 regions for USTR. SSH = sea surface height; SST = sea surface temperature; USTR = zonal wind stress.

170° to 120°W, respectively) in the Atlantic and Pacific for both SSH and SST; and into the WAtl and Nino4 regions (3°S to 3°N, 40° to 20°W, and 5°S to 5°N, 160°E to 150°W) for USTR. The data sets agree well with each other, and anomaly correlation values between pairs of time series of the same variable all exceed values of 0.9. Additionally, Figure 1 highlights differences between the Atlantic and Pacific Niños (see section 1). It is obvious that Pacific Niño events have a distinct signature in the anomaly time series of SSH, SST, and USTR, being characterized by intermittent, strong events that are clearly phase-locked to boreal winter (Figures 1a, 1e, and 1i). In contrast, variances in the Atlantic are much smaller and events occur more regularly, producing anomaly time series that resemble white noise (Figures 1b, 1f, and 1j). Figures 1k and 1l indicate that the ERA-Interim and ORAS4 USTR data are not exactly equal, although they are both ERA products. This could be due to the blending in ORAS4, and to a lesser degree to the different horizontal resolutions of the two data sets, with ORAS4 USTR being higher resolved than the ERA-Interim data used in this study.

2.2. Estimating the Strength of the Bjerknes Feedback Elements

We use robust regression to diagnose the strength of individual Bjerknes feedback elements (Huber & Ronchetti, 2009; Holland & Welsch, 1977; Street et al., 1988). In statistical analysis, developing a model of a given data set requires assumptions about the processes that generated the data. Ordinary least squares-based linear regression (OLS) can be unreliable when these assumptions are violated, especially in the presence of outliers, since OLS minimizes the squared distances between the original data and the guess of the prediction. Robust regression techniques—a collection of methods that seek to lessen the sensitivity of the regression coefficients to outliers—generally change the weight that is attributed to each residual

when considering its impact on the final regression coefficients. A common approach is to assign a relatively strong weight to small residuals, and decrease the weight of large residuals that are likely associated with outliers. While robust regression has been designed with outliers in mind, Zheng et al. (2014) demonstrated that it is a valid way to perform regression analysis based on small data sets in climate science. We adopt this approach here, using Matlab's implementation of robust regression (`robustift`, current documentation provided by `https://de.mathworks.com/help/stats/robustfit.html`). For our analysis, we use the default `robustfit` of Matlab's 2018 distribution, which iteratively reweights least squares with a bisquare weighting function.

To diagnose the strength of the Bjerknes feedback elements in our zonal analysis, we average equatorial SSH and SST into 4° longitude × 4° latitude boxes that slide along the equator. Zonal wind stress (USTR) is fixed to WAtl in the Atlantic, and Nino4 in the Pacific, since it is the western basin wind stress that dominantly contributes to the closed Bjerknes feedback and not the local wind stress.

As in the case of OLS, robust regression, too, assumes a linear relationship between the two variables that are related to each other. In the tropical Atlantic, Lübbecke and McPhaden's (2017) show a fairly linear relationship for all elements of the Bjerknes feedback (see their Figure 3). In the equatorial Pacific, on the other hand, a number of studies have shown that nonlinear processes affect the variability associated with the Pacific Niño (Dommenget et al., 2013; Takahashi & Dewitte, 2016; Timmermann et al., 2018). These processes, however, usually serve to explain the strongest events or the overall asymmetry between warm and cold events (see section 1). Here, we recognize the overall asymmetries and are interested in a canonical analysis of the Bjerknes feedback associated with the Pacific Niño. Because of this, and for the sake of direct comparability between the Atlantic and Pacific basins, we have decided to apply the same (linear) analysis to both ocean basins.

2.3. Including Lagged Feedback Elements Into the Analysis

Unless stated otherwise, we take into account that any of the Bjerknes feedback elements could be lagged when we calculate composite strengths in this study (see section 2.4 for details on the feedback element composites). To identify lags, we use robust regression to conduct a cross-regression analysis prior to diagnosing the composite strengths for each analysis period. During the cross-regression analysis, we fix the forcing variable of the feedback element—the variable that "drives" the feedback element, that is, SSH, SST, and USTR for the SSH-SST, SST-USTR, and USTR-SSH feedback elements—to our analysis month and shift the month at which the response variable is measured for up to ±8 months. Negative lags indicate that the relationship is strongest when the response variable leads the forcing variable. In this case, the causality of the three relationships forming the Bjerknes feedback is severed. For this reason, we will discard results associated with negative lags for the remainder of the study.

Figure 2 shows the lags that our cross-regression analysis identified, for the OBS data set group and the period 1993–2012. To produce the results shown in section 3, we assume that the lags are independent of the subset of data that was used to diagnose them (see section 2.4). In section A1 of the Appendix, we discuss the validity of this assumption and find that it generally holds. However, this assumption can *locally* degrade the strength of the feedback element, demonstrating again how diverse the mechanisms are that produce the variability of the Atlantic and Pacific Niños and that it may not be justified to make equivalent assumptions for warm and cold events.

Figure 2 shows that in the Pacific, all feedback elements are generally characterized by positive lags that start to occur in May and decrease until boreal winter, indicating that the closed feedback loop becomes more instantaneous in the latter half of the year (Figures 2a–2c). Zonal variations are small, and lags tend to occur uniformly across large parts of the Pacific.

In the Atlantic, lags associated with subsurface-surface coupling are generally positive (Figure 2d), indicating that SSH leads SST variability by 3 months at most. During June and July, and again in boreal winter, lags vanish and subsurface-surface coupling becomes instantaneous. The SST-USTR and USTR-SSH feedback elements, on the other hand, are characterized by lags ≥0 only during spring and early summer, and again during boreal winter. In agreement with Keenlyside and Latif's (2007) and Burls et al.'s (2011) studies on the seasonality of the Atlantic Bjerknes feedback, this indicates that the Bjerknes feedback can only establish a closed feedback loop during early summer and winter. Another feature of Figures 2d–2f is that the lags of the feedback elements are not distributed evenly across the zonal extent of the basin. Rather, pos-

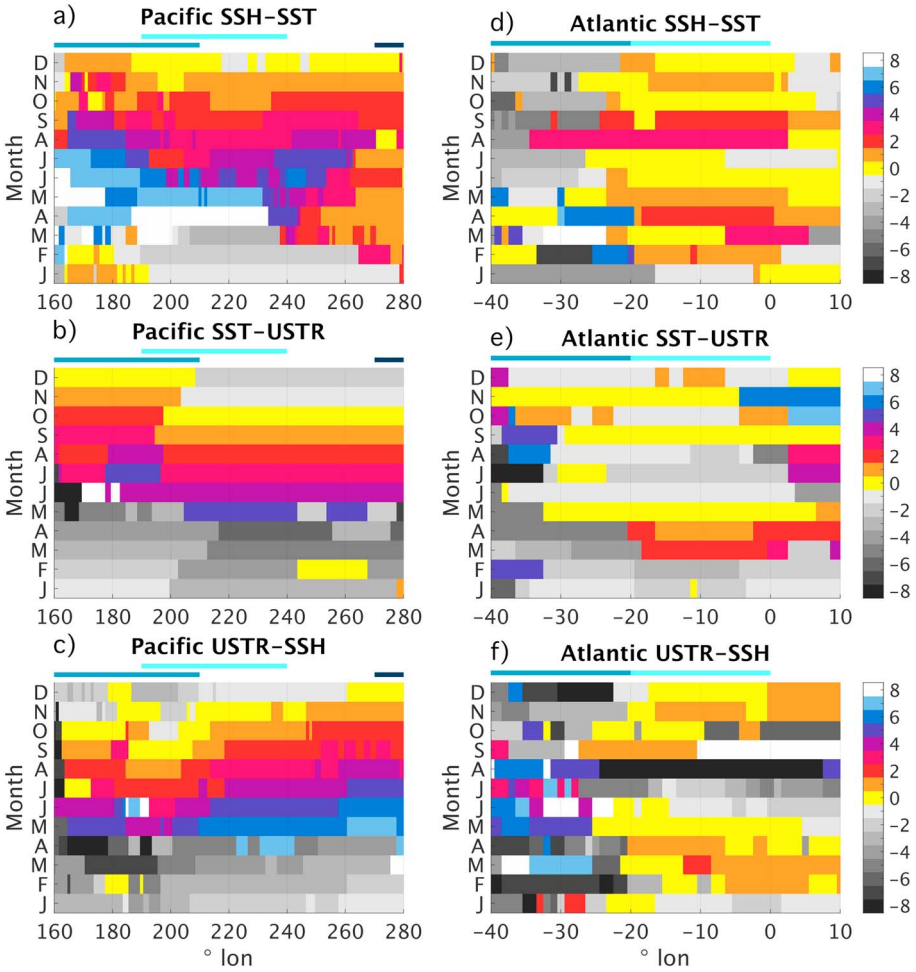

Figure 2. Lag in months at which the relationship for each of the three Bjerknes feedback elements is strongest. Data are shown along the equator (*x* axis) and stratified into calendar months (*y* axis) for both the Pacific (left column, panels a–c), and the Atlantic (right column, d–f). The sign of the lag is with respect to the forcing variable of the feedback element, that is, SSH, SST, and USTR for the SSH-SST, SST-USTR, and USTR-SSH feedback elements, respectively. A positive lag indicates that the forcing variable leads the response variable. Positive lags are shown in color, with a lag of zero months indicated by yellow. Negative lags are shown in gray shading. The top, middle, and bottom rows show results for subsurface-surface coupling (a,d), SST-wind coupling (b,e), and wind-thermocline coupling (c,f). For each longitude, data have been averaged into 4° longitude × 4° latitude bins prior to calculation. This binning has been done for each analysis, unless stated otherwise. Colored bars below the titles indicate the zonal extent of the Nino4, Nino3.4, and Nino1.2 (WAtl and Atl3) regions in the Pacific (Atlantic) in blue, light blue, and dark blue (blue and light blue). SSH = sea surface height; SST = sea surface temperature; USTR = zonal wind stress.

itive lags occur predominantly in or close to the Atl3 region, showing that the Atlantic Bjerknes feedback is constrained not only to two short periods but also to a narrow spatial domain.

We include lags into our robust regression analysis by shifting the time series of the response variable according to the identified lag.

2.4. Assessing the Symmetry of the Bjerknes Feedback: Compositing Feedback Elements

To assess the symmetry of a Bjerknes feedback element, we partition it into positive and negative composites. Note that we do *not* separate our feedback elements into consistent warm/cold composites according to SST conditions, but rather assign individual composites to each feedback element, based on its forcing variable.

Figure 3 illustrates this two-step decomposition of the Bjerknes feedback loop—into feedback *elements* first, then into *composites* of the feedback elements—and lists how negative and positive composites of each feedback element can be interpreted in terms of the forcing variable. Because of the partitioning of our base data pool into positive and negative composites prior to our regression analysis, the effective sample sizes for our

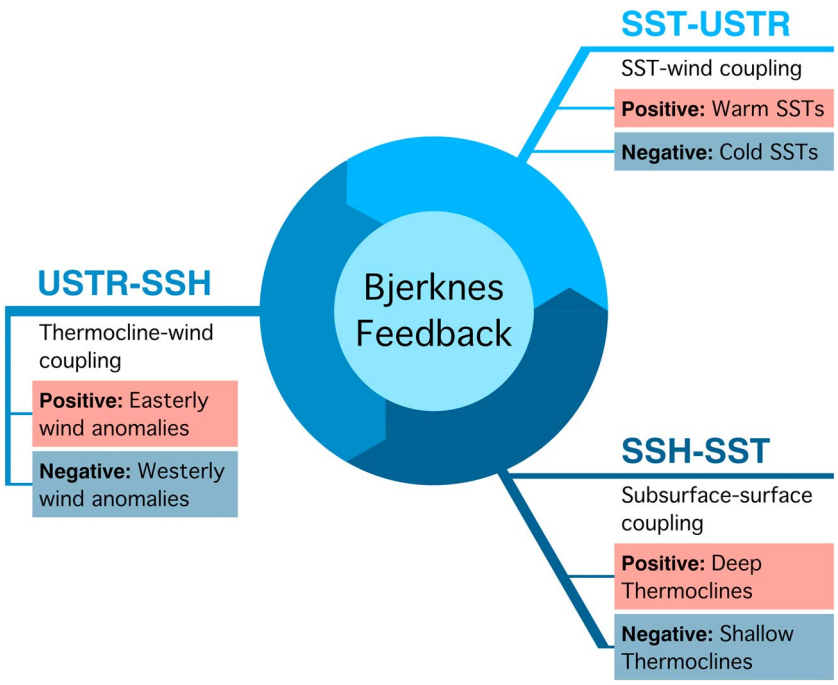

Figure 3. Schematic of the feedback decomposition approach. The closed Bjerknes feedback loop is decomposed into three interacting *feedback elements* (partitioned ring around the central circle). These feedback elements are the subsurface-surface coupling (SSH-SST, dark blue, bottom right), SST-wind coupling (SST-USTR, light blue, top right), and wind-thermocline coupling (USTR-SSH, blue, left). Each feedback element is additionally partitioned into two *composites* (red and blue boxes below each feedback element). Composites are based on the sign of the anomalies of the forcing variable, that is, SSH, SST, and USTR for the SSH-SST, SST-USTR, and USTR-SSH feedback elements, respectively. The text in the composite boxes explains how each composite can be interpreted with respect to its "parent" feedback element (see section 2.4). SSH = sea surface height; SST = sea surface temperature; USTR = zonal wind stress.

robust regression are on the order of 10 for the period 1993–2012 (section 3), and 12 for the 25-year periods considered in section 4. This is a very small sample size. Even though we employ robust regression, we will refrain from attributing too much value to individual numbers and will rather focus on general patterns.

2.5. Bootstrapping Significances

Significance in our study indicates that a given composite of a feedback element (or their difference) is significantly different from the expected strength (difference) of that feedback element when it is diagnosed from a random subsample of the data. We estimate this significance using a simple bootstrapping approach outlined below.

For a (strength) composite of a Bjerknes feedback element, we generate a distribution of the expected feedback element strength by rediagnosing the robust regression coefficients for random subsamples of the full data pool. Subsamples ignore composites, but have the same sample size as the composites they test and obey the same lags (see Figure 2). By iterating through a large number of subsamples, we bootstrap a distribution of pseudo-composite strengths, whose expected value corresponds to the relationship strength of the feedback element when the data is not partitioned into composites. Next, we use the bootstrapped distribution to perform a simple significance test. If the composite strength is outside the 90% area of the bootstrapped distribution for a significance level of $\alpha = 0.1$ and the case of a one-sided test, we reject the null hypothesis that the composite strength is equal to the relationship strength based on the full data set. The composite strength is significant.

For the difference between the positive and negative composites, we repeat the above method, but use the difference between the calculated composite strengths as the target of the test, instead of the absolute composite strength. For this, we again determine the size of our subsample, randomly draw a new sample of the same size, and use the remaining data in the pool as the pseudo-counter composite. In both cases, we perform 1,000 bootstraps and use a significance level of 0.1.

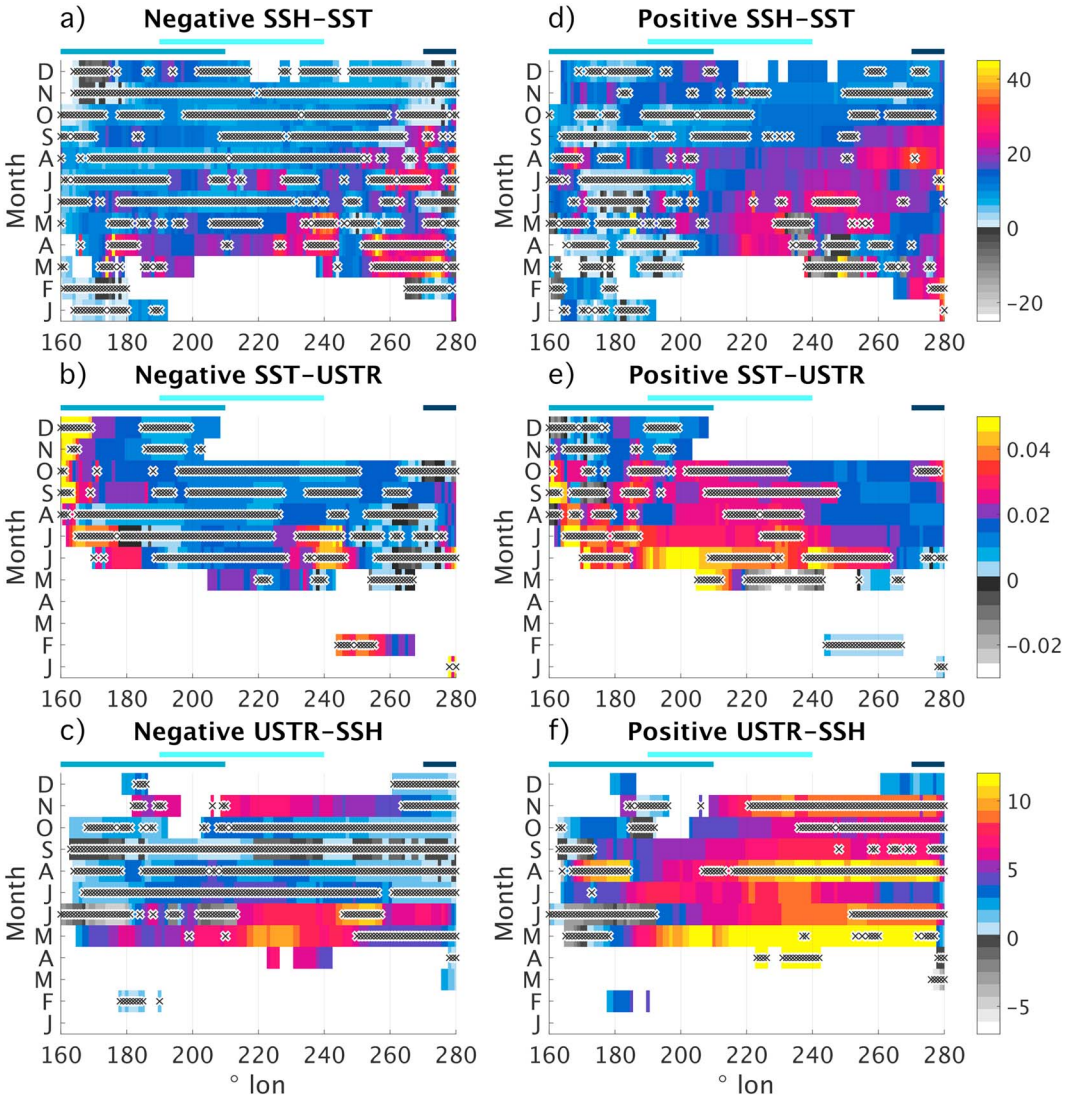

Figure 4. Composites of the OBS-based feedback elements in the Pacific, for the recent period 1993–2012 along the equator (*x* axis) and stratified into calendar month (*y* axis) with respect to the forcing variable. The top, middle, and bottom row show results for the SSH-SST (panels a, d), SST-USTR (b, e), and USTR-SSH feedback elements (c, f), with forcing variables SSH, SST, and USTR, respectively. To estimate the sensitivity of the two involved variables for the case of either positive or negative anomalies of the forcing variable, cf. section 2.4, we use the slope parameter provided by robust regression. Color shading indicates positive values, with small values shown in blue, and the highest values shown in reds and yellows. Negative values, indicating that a feedback element disrupts the closed Bjerknes feedback, are shown in gray shading, with the lightest greys indicating the largest negative values. White indicates that, at the given longitude and month, the lag diagnosed in Figure 2 is negative and hence is not in agreement with the framework of the Bjerknes feedback. Sensitivities are given in units of K/m, N/(m^2 K), and m^3/N for the three feedback elements, respectively. The left and right columns show the sensitivities for the negative (a–c) and positive composites (d–f). Significance is indicated by black crosses with a white outline (see text for details). Colored bars below the title indicate the zonal extent of the Nino4, Nino3.4, and Nino1.2 regions in blue, light blue, and dark blue, respectively. SSH = sea surface height; SST = sea surface temperature; USTR = zonal wind stress.

3. Symmetry of the Atlantic and Pacific Bjerknes Feedbacks 1993–2012

3.1. Bjerknes Feedback Element Strengths

To validate our method of partitioning the strength of the Bjerknes feedback elements into positive and negative composites, we discuss our results based on the OBS data set group for the Pacific (Figure 4, differences shown in Figures 5a–5c). We use the lags shown in Figure 2.

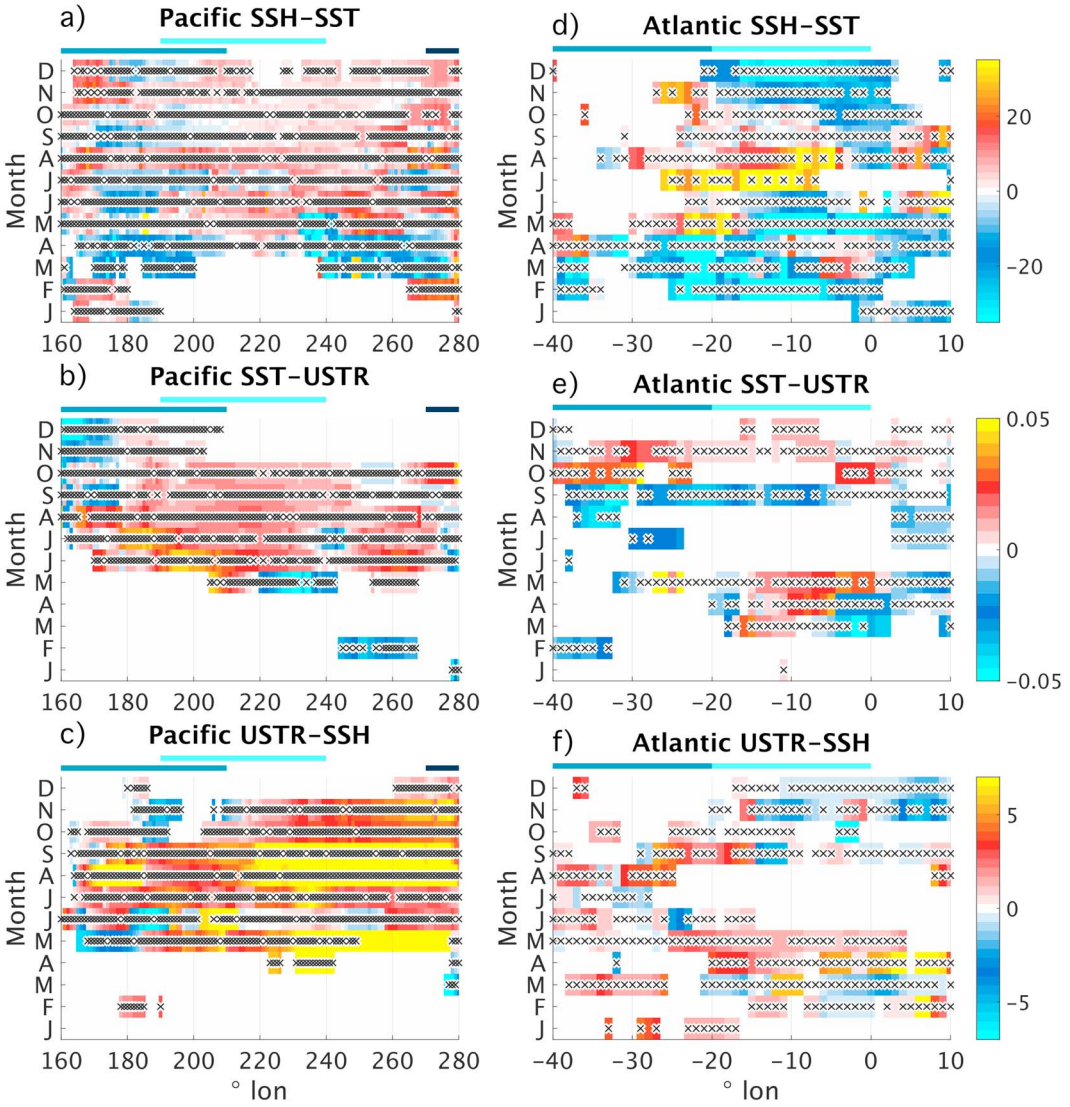

Figure 5. Similar to Figure 4, but showing the difference between positive and negative composites of the feedback elements in the Pacific (left column, panels a–c) and the Atlantic (right column, d–f), for the SSH-SST (a, d), SST-USTR (b, e), and USTR-SSH (c, f) feedback elements. Blue (red-yellow) shading indicates that the negative composite is larger (smaller) than the positive composite. Colored bars below the titles indicate the zonal extent of the Nino4, Nino3.4, and Nino1.2 (WAtl and Atl3) regions in the Atlantic (Pacific) in blue, light blue, and dark blue (blue and light blue). SSH = sea surface height; SST = sea surface temperature; USTR = zonal wind stress.

In agreement with the equatorial Pacific "spring barrier," both the composites of the SST-USTR and USTR-SSH feedback elements decline during late boreal winter and spring in the Pacific (Figures 4b–4c and 4e–4f). The spring barrier is a concept that originates from seasonal predictability studies and refers to the drop in predictability of the Pacific Niño during boreal spring (Duan & Wei, 2013; Torrence & Webster, 1998). Wengel et al. (2018) showed that the spring barrier is associated with a weakening of the atmosphere-ocean coupling in the tropical Pacific, which temporarily decreases the strength of the Bjerknes feedback estimated by Jin et al. (2006)'s Bjerknes stability index (see section 5). Our results confirm this.

In the Nino3.4 region and the eastern ocean basin, negative composites are significantly different from the expected relationship strength more frequently than positive composites. This is shown by the distribution of significance, indicated by overlaid black crosses in Figure 4. The dominance of positive events over negative events is in agreement with previous studies on Pacific Niño asymmetries. In particular, while cold events are rather modest in magnitude, virtually all extreme events are warm and hence strongly shape the overall characteristics of the Pacific Niño (note, however, that really only one "extreme event" occurred in the short

period 1993–2012). Consequently, the positive composites of the feedback element strengths are in better agreement with the expected overall relationship strengths than the negative composites.

Pacific subsurface-surface coupling (Figures 4a and 4d) is positive for almost the entire year and across most of the Pacific basin. East of 150°W (210°E), the positive composite is generally stronger than the negative composite (Figure 5a), in particular, in the far eastern basin during late boreal summer, coinciding with the main onset phase of warm Pacific Niño events.

Pacific SST-wind coupling, too, is generally stronger for the positive composite (Figures 4b, 4e, and 5b). Physically, this could be due to a threshold dependence of equatorial deep convection. While warm SST anomalies promote overlying convection effectively, cold SSTs do not necessarily suppress convection to the same degree (Levine & Jin, 2017). Consequently, wind variability is more sensitive to warm SST anomalies than to cold SST anomalies.

An interesting feature of the positive composite of the Pacific SST-USTR feedback element is that it is strongest in the central Pacific (Figure 4e)—it seems to operate more locally in our analysis framework than expected (this, however, could be a consequence of USTR being fixed to the western ocean basin). The strength of the positive feedback element peaks just after the collapse of the spring barrier in early boreal summer, when a clear asymmetry between the negative and positive composites emerges. This asymmetry persists into boreal winter and is strongest in the Nino3.4 region (Figure 5b). SST-wind coupling stops contributing to a closed Bjerknes feedback in November for both composites (Figures 4b and 4e, and lags shown in Figure 2b).

Last, Figures 4c, 4f, and 5c indicate that Pacific wind-thermocline coupling is highly asymmetric for the second half of the year, especially in the eastern portion of the basin. Again, the feedback element is strongest after the collapse of the spring barrier. The zonal distribution of the feedback strength composites indicates that the Nino4 wind stress indeed is strongly related to thermocline variability in the central and eastern ocean basin, in good agreement with the Bjerknes feedback framework.

Overall, the elements of the Pacific Bjerknes feedback display a clear asymmetry. Positive composites are generally stronger than negative composites, especially in the eastern ocean basin when SSH is involved. Simultaneously, negative composites are more frequently significantly different from the overall expected relationship strength, indicating that the characteristics of the Pacific Bjerknes feedback elements are largely shaped by the positive composites. These findings are in excellent agreement with previous studies on Pacific Niño asymmetries and demonstrate that our lagged, robust regression-based feedback analysis is well suited to investigate feedback asymmetries in an equatorial ocean basin.

A peculiar finding is that our lagged feedback strengths appear to be phase-locked to early boreal summer rather than winter. While the feedback elements do persist into boreal winter, they are strongest in summer. This suggests that the weak spring coupling very rapidly turns into effective coupling that organizes incipient anomalies in the atmosphere and the ocean into the Bjerknes feedback. During the peak phase of the Pacific Niño these feedback elements are still active, but they are weaker than during the initial growth phase in boreal summer. On the one hand, these findings seem to be at odds with a number of previous studies, including Zhu et al.'s (2015) discussion of the seasonality of Pacific subsurface-surface coupling (their "thermocline feedback"). They report that instantaneous subsurface-surface coupling is weakest in March, and then gradually increases until it peaks in October and November. However, their study does neither explicitly consider lags nor does it distinguish between "deep" and "shallow" thermocline depths as we do here. On the other hand, recent work by Wengel et al. (2018), supported by early work by Zebiak and Cane (1987), suggests that atmosphere-ocean coupling in the tropical Pacific indeed is strongest in late boreal spring and early summer, in agreement with our findings. The discrepancies between these studies and our findings will have to be resolved by future research.

Next, we present our results for the Atlantic Bjerknes feedback (Figures 5d–5f and 6). In agreement with Lübbecke and McPhaden (2017), the range of the feedback element strengths is generally comparable to the Pacific, except for the weak Atlantic wind-thermocline coupling (Figures 6c and 6g). In addition to the weak sensitivity between USTR and subsurface variability, the following factors are commonly discussed to explain the muted amplitude of the Atlantic Niño relative to the Pacific Niño. First, the zonal extent of the Atlantic is much smaller than that of the Pacific, which could constrain the fully coupled feedback. Second, the Bjerknes feedback operates on shorter time scales in the Atlantic, effectively coupling the atmosphere

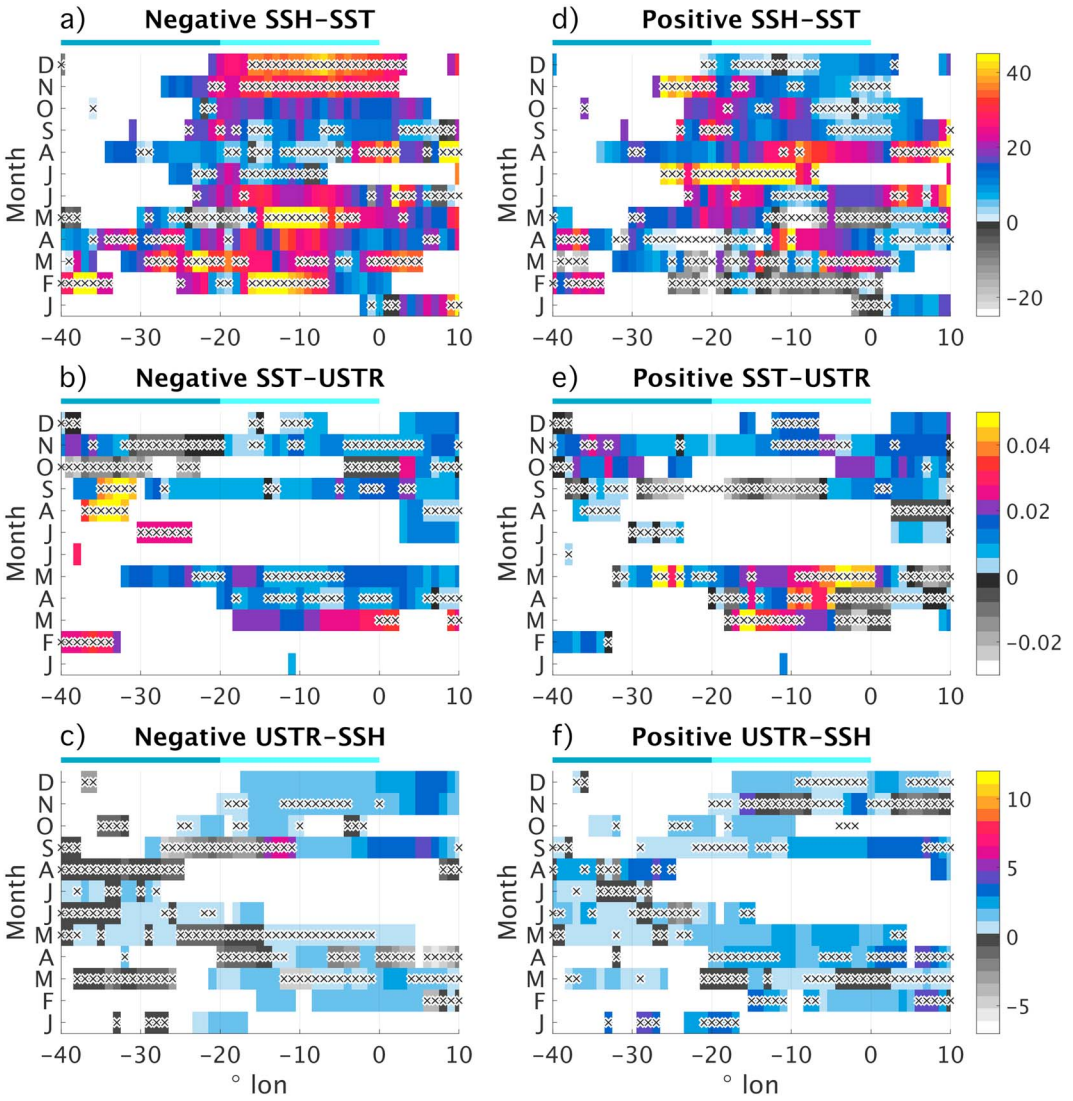

Figure 6. Same as Figure 4 but for the Atlantic. Colored bars below the title indicate the zonal extent of the WAtl and Atl3 regions in dark and light blue, respectively. SSH = sea surface height; SST = sea surface temperature; USTR = zonal wind stress.

and the ocean for only 2 to 3 months in a row at best and hence diminishing the amplitude that anomalies can grow to. This is consistent with our analysis.

Atlantic subsurface-surface coupling appears to be the dominant element of the Atlantic Bjerknes feedback (Figure 6). Clear asymmetries emerge throughout boreal summer and early winter (Figure 5d). In boreal summer, during the peak season of the summer Niño, the negative composite is stronger until July; for the remainder of boreal summer and early fall, the positive composite contributes more effectively to the overall feedback element. This suggests that subsurface-surface coupling sets in earlier for cold Atlantic Niño events. (While it is tempting to argue that the SSH-SST feedback element should naturally be stronger for shallow thermoclines due to the enhanced sensitivity of SST to small changes in thermocline depth, this reasoning clearly breaks down in the equatorial Pacific, where subsurface-surface coupling is strongest for deeper-than-normal thermoclines, cf. Figure 5d. A possible explanation for this is that shallow thermoclines have to outcrop at some point, capping the maximum strength of the negative SSH-SST feedback element, while the thermocline can deepen more or less without constraints for the positive SSH-SST composite.) In boreal winter, the negative composite reemerges, while the positive composite is practically absent. The overall seasonality of Atlantic subsurface-surface coupling is in good agreement with our understanding

of the Atlantic Niño. An interesting side note is that the Atlantic SSH-SST feedback element appears to be stronger than its Pacific counterpart when it peaks (cf. Figures 4a, 4d, 6a, and 6d).

Atlantic SST-wind coupling, on the other hand, appears to be weaker than its Pacific counterpart (cf. Figures 4b, 4e, 6b, and 6e). Nevertheless, consistent asymmetries arise between positive and negative composites. In agreement with the enhanced sensitivity of wind variability to warm SST anomalies discussed for the Pacific SST-USTR feedback element, the positive composite is generally stronger than the negative composite. However, the lags that we used to diagnose the Atlantic SST-USTR feedback element are negative from June to September (Figure 2f) and SST-wind coupling hence only really contributes to a closed Bjerknes feedback loop in May. This limited contribution of the SST-USTR feedback element indicates that equatorial wind variability is less sensitive to ocean variability in the Atlantic than in the Pacific.

Last, Atlantic wind-thermocline coupling is clearly weaker than its Pacific counterpart (Figures 6c and 6f). In the case of the negative composite, it changes from being weakly positive to negative in August, indicating that it blocks anomaly growth and hence effectively contributes to the breakdown of the Atlantic Bjerknes feedback. This agrees with Dippe et al. (2018), who show that the closed Atlantic Bjerknes feedback collapses in August. Differences between the negative and positive composites are generally small, with the positive composite prevailing slightly. (The substantial difference in August is of no practical concern, since even the apparently overwhelming positive composite is only weakly positive in absolute terms, cf. Figure 6f.) Similar to the SST-wind coupling discussed above, wind-thermocline coupling, too, can only contribute to a closed Bjerknes feedback in early boreal spring and winter, when the lag relationships are positive.

Overall, we identified asymmetries for all Atlantic Bjerknes feedback elements. These asymmetries occur mainly in boreal summer and are most pronounced for the SSH-SST feedback element associated with subsurface-surface coupling. The two feedback elements that involve wind variability produce a less straightforward picture. They are weaker than their Pacific counterparts and constrain the Atlantic Bjerknes feedback to boreal summer and winter. This rather disruptive wind variability and decreased wind sensitivity to SST is in agreement with previous studies on the Atlantic Niño. A physical explanation of this difference between the Pacific and Atlantic Niños could be linked to the small zonal extent of the Atlantic, which substantially decreases the "fetch" of the wind stress variability in comparison to the Pacific. Additionally, enhanced interference, for example, from midlatitudes or the tropical Pacific, could explain why wind plays a somewhat different role for the Atlantic.

3.2. The Total Bjerknes Feedback

In section 3.1, we have demonstrated that both the Atlantic and Pacific Bjerknes feedback elements can be asymmetrical. Here, we attempt to combine our findings for the individual feedback elements and assess how symmetric the overall effect of the closed Bjerknes feedback loop is for warm and cold conditions in the central equatorial ocean basin. We call this integrative measure the total Bjerknes feedback.

We diagnose the total Bjerknes feedback by adding the strengths of the instantaneous feedback elements of the positive and negative composites. Instantaneous feedback elements are calculated in the same manner as lagged feedback elements, but use a constant lag of zero months, that is, the two time series contributing to each strength estimate have been sampled at the same calendar month. We use instantaneous feedback elements to avoid running into timing discrepancies.

Our approach of adding up the strength composites of the individual Bjerknes feedback elements is much simpler than the existing framework of Jin et al.'s (2006) Bjerknes stability (BJ) index. The BJ index assesses the overall stability of the coupled equatorial system and hence its ability to support self-sustained growth of SST anomalies. The BJ index implicitly considers both processes that damp and promote anomaly growth. Damping processes are associated with mean upwelling and thermal damping; amplifying processes are the positive thermocline, zonal advection, and Ekman feedbacks. Our analysis, on the other hand, is confined to the framework of the positive, anomaly-growth-promoting Bjerknes feedback.

In contrast to the Bjerknes feedback elements shown in Figures 4 and 6, the total Bjerknes feedback corresponds to warm and cold SSTs in the equatorial ocean basin. See section A2 of the Appendix for the total Bjerknes feedback associated with westerly/easterly wind anomalies or with deep/shallow thermoclines, or for the case using the "native" composites of each feedback element.

For the previous analysis, our estimate of the composite strengths was the regression parameter that we obtained from robust regression. This method produced strength estimates that preserved a meaningful

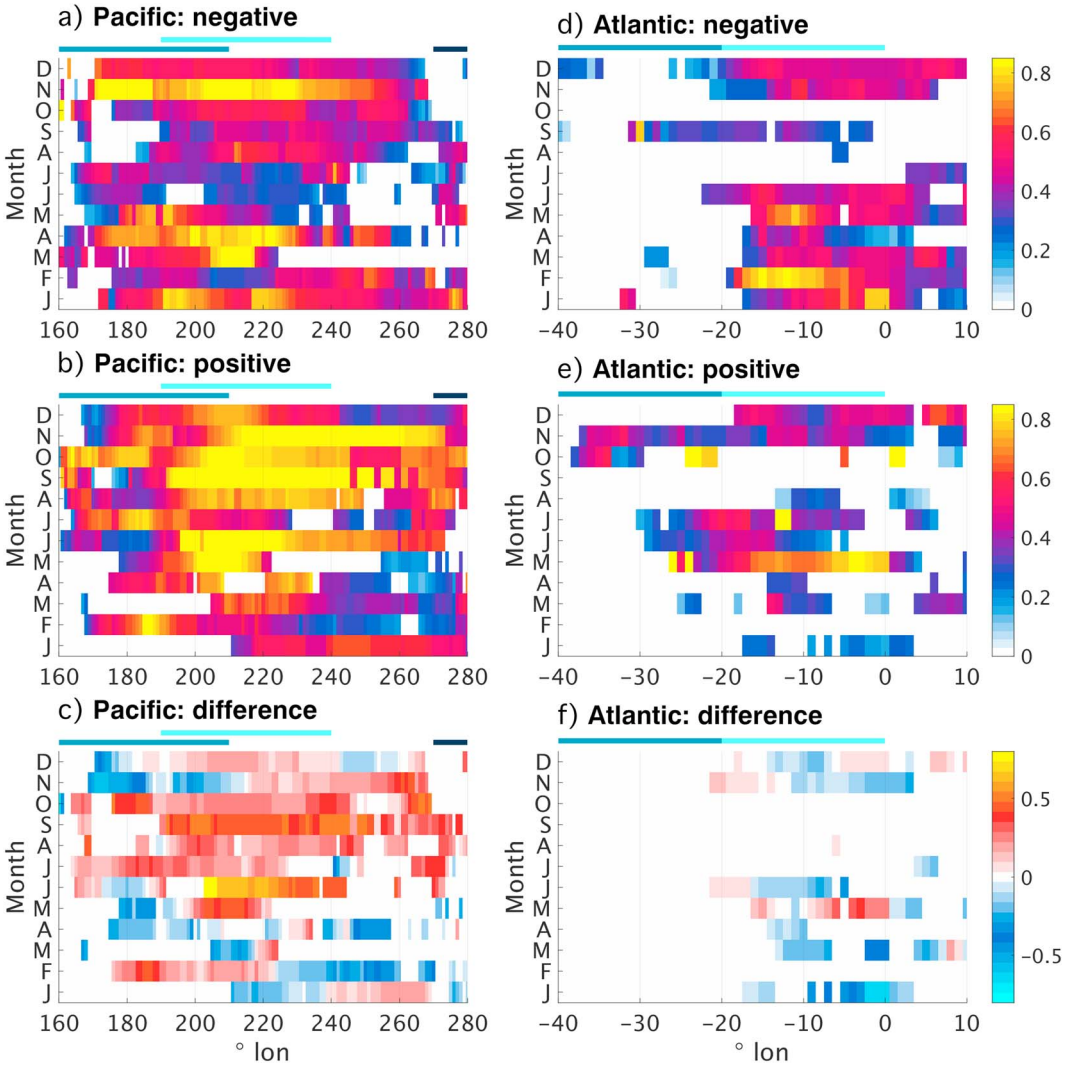

Figure 7. SST-based estimate of the total Bjerknes feedback during 1993–2012 in the Pacific (a–c) and Atlantic (d–f), along the equator (*x* axis) and stratified into calendar months (*y* axis), diagnosed for the OBS dataset group. The top, middle, and bottom rows show the total of all negative composites (a, d), the total of all positive composites (b, e), and the difference between the positive and negative composites of the total Bjerknes feedback (c, f), respectively. Feedback strengths of the individual Bjerknes feedback elements have been normalized with 60 K/m, 0.075 N/(m^2 K), and 11 m^3/N for the SSH-SST, SST-USTR, and USTR-SSH feedback elements, respectively. All feedback elements have been diagnosed without considering lag, and for each composite, they all use the same subsample of the data. These composites were diagnosed from the sign of the SST anomaly. Hence, the positive and negative composites of the total feedback assess the strength of the Bjerknes feedback when SSTs are warm or cold, respectively. The composites of the total feedback are the sum of all normalized composites. See text for additional details on how the total Bjerknes feedback was computed. White indicates that at least one of the feedback elements was negative, that is, that the Bjerknes feedback loop was not closed. For the difference plots (c, f), white indicates that at least one feedback element was negative in *either* of the positive or negative composites. SSH = sea surface height; SST = sea surface temperature; USTR = zonal wind stress.

physical unit. Now, we normalize our feedback strengths to constrain them to values between −1 and +1, without units. For the normalization in both the Atlantic and the Pacific basins, we use the values 60 K/m, 0.075 N/(m^2 K), and 11 m^3/N for the SSH-SST, SST-USTR, and USTR-SSH feedback elements, respectively. Strength estimates whose magnitude exceeds these "cutoff values" are set to ±1, depending on their sign. The cutoff values were chosen such that, based on all diagnosed strengths of the same composite in both basins, the magnitude of 95% of all values are smaller or equal to the cutoff value. Last, we average all normalized feedback strengths contributing to the same composite and obtain composites of the total Bjerknes feedback with respect to cold and warm SSTs.

Figure 7 shows the total feedback according to our simple measure. Instances where the feedback loop is "broken" by a single feedback element contributing negative values and hence inhibiting anomaly growth are shown in white.

In agreement with previous studies, the total (instantaneous, SST-based) Pacific Bjerknes feedback is dominated by contributions from its positive composite, that is, it is stronger for warm SSTs (Figures 7a–7c). The feedback forms a closed loop for practically the entire year, indicating that feedback-driven anomaly growth can be active for much of the year. A clear, common seasonality for both the cold and warm composites does not exist. The cold composite is weakest in boreal summer, while the warm composite is diminished at the beginning of the calendar year, indicating that the spring barrier affects positive and negative composites in a slightly different fashion. An interesting detail in the distribution of the composite totals is that the Bjerknes feedback is not closed in the negative composite in the far eastern basin, not even during the peak time of the Pacific Niño in boreal winter. This is in agreement with studies on different regimes of the Pacific Niño arguing that negative Pacific Niño events (La Niñas) tend to develop in the central basin and hardly ever manifest in the far eastern basin in their extreme form (Capotondi et al., 2015; Dommenget et al., 2013; Takahashi et al., 2011; Takahashi & Dewitte, 2016).

In contrast to the Pacific, the total Atlantic Bjerknes feedback displays a pronounced seasonality (Figures 7d–7f). Both the warm and cold composites are generally strong in summer and early boreal winter, but almost vanish in-between. However, Figures 7d and 7e show that the timing and magnitude of these seasonal peaks is different for the warm and cold composites—asymmetries emerge in the total Atlantic Bjerknes feedback.

During boreal summer, the cold composite is strongest in May and June, while the warm composite lasts a month longer. This agrees with Burls et al. (2012), who argued that cold summer Niño events are associated with an early onset of the cold tongue, while cold tongue development is delayed during warm events. In boreal winter, cold SST anomalies feed coupled anomaly growth in late winter, while warm SST anomalies lend little support to anomaly growth. These results suggest that the Bjerknes feedback supporting the Atlantic summer Niño relies on contributions from both cold and warm conditions. The winter Niño and possible coupled variability during the first months of the year, on the other hand, is mainly associated with negative SST anomalies, at least within the framework of the Bjerknes feedback.

4. Stationarity of the Bjerknes Feedback

The results of the previous section for the Atlantic appear to be at odds with the results of Lübbecke and McPhaden (2017). One core result of their study is that the SST anomalies associated with warm and cold Atlantic Niño events are effectively mirror images of each other and that the associated, seasonal Bjerknes feedbacks appear to be symmetric as well. While Lübbecke and McPhaden (2017) find a weak disparity for the positive and negative composites of the strength of subsurface-surface coupling, this asymmetry is not comparable to the pronounced asymmetries associated with the Pacific Niño. Lübbecke and McPhaden (2017) base their analysis on the approximately 50-year period 1958–2009 and diagnose feedback strengths using data of at least 2 months, allowing for lags of 1 month between the involved time series.

Our data situation is different. The OBS data set group spans the 20-year period 1993–2012, and we have chosen to resolve our results as highly as possible, taking into account month-to-month variations and a possible dependence on longitude as well.

To facilitate a direct comparison and assess the robustness of our results, we calculate the index-based monthly composite strengths of all feedback elements for the overlap period of the OBS and ORAS4 data set groups 1993–2009 (Figure 8). The feedbacks are calculated in the same manner as above but use indices that are averaged over the Atl3/WAtl and Nino3.4/Nino4 regions in the Atlantic and Pacific for SSH and SST/USTR, respectively. Lags are rediagnosed for the period 1993–2009 and incorporated in the same manner as in section 3.

Agreement between the two data set groups is excellent in the Pacific (Figures 8d–8f). Timing is mostly congruent, apart from the very sharp drop in the positive composite of the SST-USTR feedback element that occurs in May in the OBS, and in April in the ORAS4 data set group, consistent with the spring barrier. Additional smaller discrepancies are apparent for wind-thermocline coupling while preserving the overall seasonal structure of the two composites.

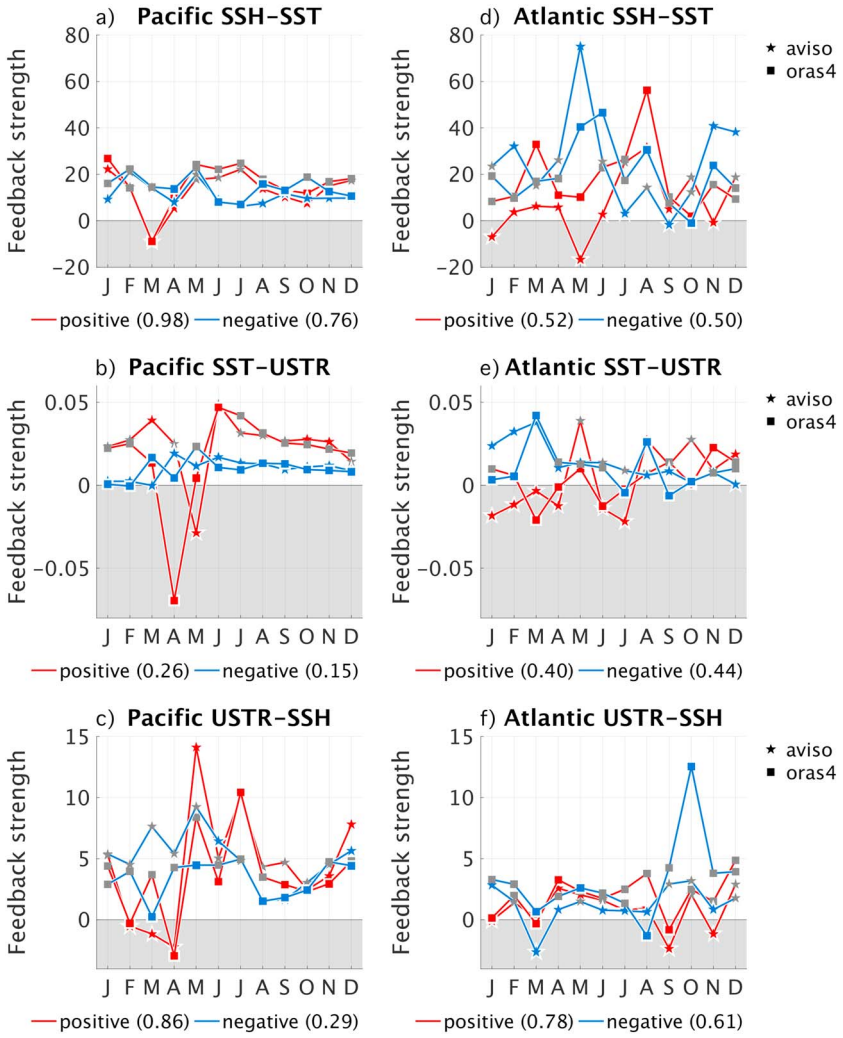

Figure 8. Comparison of feedback element composites in the OBS and ORAS4 data set groups in the Pacific (left column, a–c) and Atlantic (right column, d–f) for the overlap period 1993–2009. The top, middle, and bottom rows show results for the SSH-SST, SST-USTR, and USTR-SSH feedback elements, respectively. Composites of the feedback elements have been diagnosed with respect to Atl3/WAtl in the Atlantic, and Nino3.4/Nino4 in the Pacific, for SSH and SST/USTR, respectively. Line color indicates the positive and negative composites in red and blue, respectively. Star-shaped and square line markers indicate the OBS and ORAS4 data set groups. Colored (gray) line markers show that the respective composite is (not) significant (see text for details). For the two sets of 12 values each associated with the two data set groups shown here, the resulting anomaly correlation coefficients are given in parentheses below each panel. Note, however, that correlations for small sample sizes can be unreliable. As in Figure 4, white shading indicates that the associated lags (not shown) were negative. SSH = sea surface height; SST = sea surface temperature; USTR = zonal wind stress.

In the Atlantic, discrepancies are apparent mainly for the SSH-SST and SST-USTR feedback elements. Timing in these cases can be very different. For example, the negative composite of the SSH-SST feedback element peaks in June in ORAS4, but in May in OBS. ORAS4 produces a stronger positive SSH-SST feedback element composite, however, largely preserving significances. On the other hand, the dominant features identified in section 3.1 are evident in both data sets: strong negative composites in early summer, strong positive composites in late summer, and weak positive composites during winter. In a similar fashion, small discrepancies are apparent for SST-wind coupling, while the general distribution of feedback strengths and asymmetries is present in both data set groups. In particular, the negative composite is weakest in summer and strongest in late winter, while the positive composite peaks in May.

Overall, the OBS and ORAS4 data set groups agree well in the Pacific and support the main features identified in our analysis for the Atlantic, while differing in the details there. It follows that the apparent

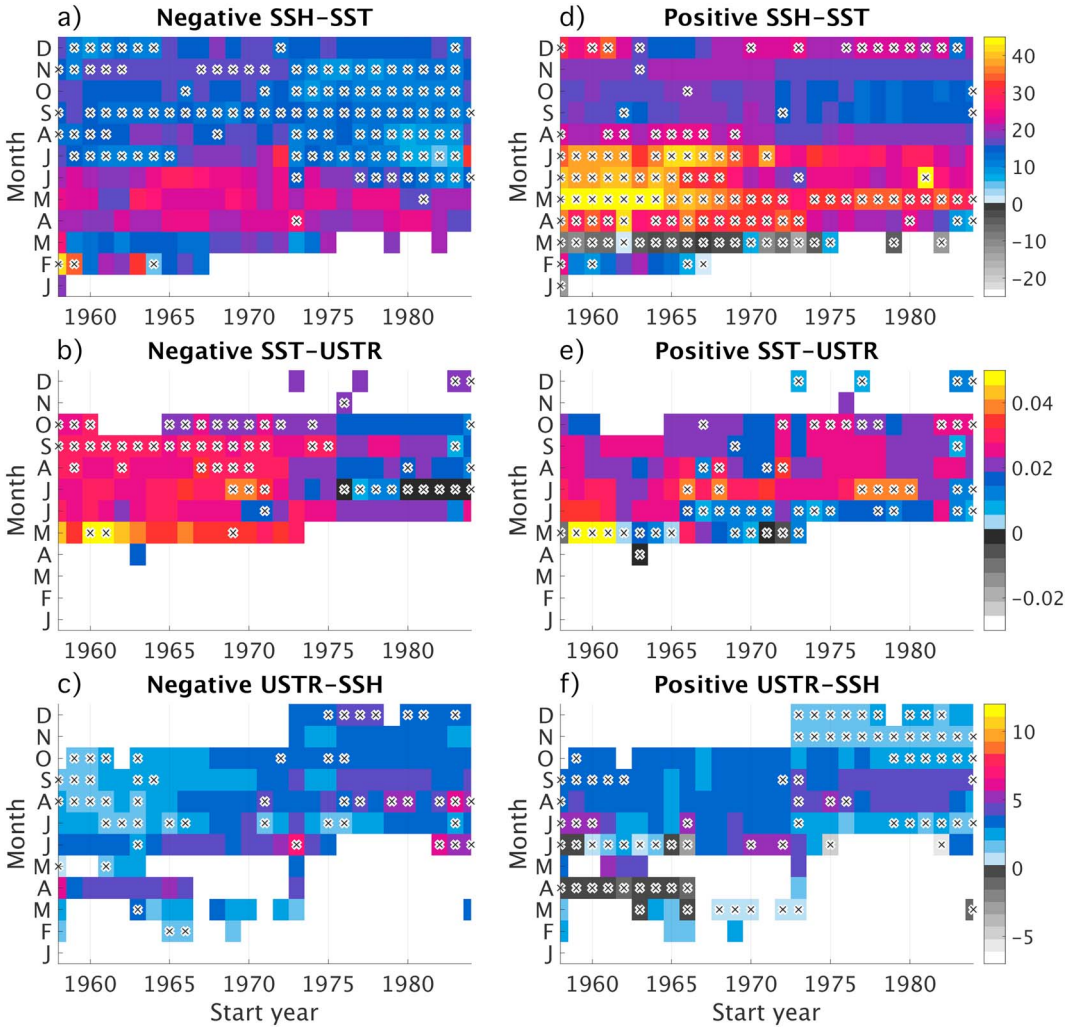

Figure 9. Decadal variations of the composites of the Pacific Bjerknes feedback elements, based on the ORAS4 data set group for running subperiods (*x* axis, shown dates label the *start* of each analysis period) and each calendar month (*y* axis). The left and right columns show variations of the negative (a–c), and positive (d–f) composites. Rows show variations of the individual feedback elements, for the SSH-SST (a, d), SST-USTR (b, e), and USTR-SSH feedback elements (c, f). Composites have been diagnosed with respect to Nino3.4 for SSH and SST, and with respect to Nino4 for USTR. Crosses indicate that the diagnosed feedback strength is significant (see text for details). Anomalies have been diagnosed with respect to the running analysis period. The width of the running window is 25 years. SSH = sea surface height; SST = sea surface temperature; USTR = zonal wind stress.

discrepancies between our work and Lübbecke and McPhaden's (2017) study must be partially attributed to the different analysis periods. In agreement with Martín-Rey et al.'s (2017) proposed nonstationarity of the Atlantic Niño itself, the Atlantic Bjerknes feedback appears to vary on decadal time scales.

To illustrate this further, we apply a "running" analysis that highlights low-frequency variations in the composite strengths of the Bjerknes feedback elements and their symmetry. For this analysis, we again use ORAS4 index data confined to the Atl3/WAtl and Nino3.4/Nino4 regions employed above. For consecutive, overlapping periods of 25 years, we rediagnose our lags and repeat our robust regression analysis, producing composites of running index-based feedback elements. Anomalies are calculated separately with respect to each period of the running analysis. This means that for each 25-year-long subperiod the data are detrended independently, and anomalies are diagnosed relative to the local seasonal cycle of each sub-period. Because both the equatorial Pacific and Atlantic basins are subject to decadal variability, this method could potentially distort our results when a common reference frame for the anomalies is required. However, repeating our analysis without detrending the data yielded practically the same results in the Pacific, and minor

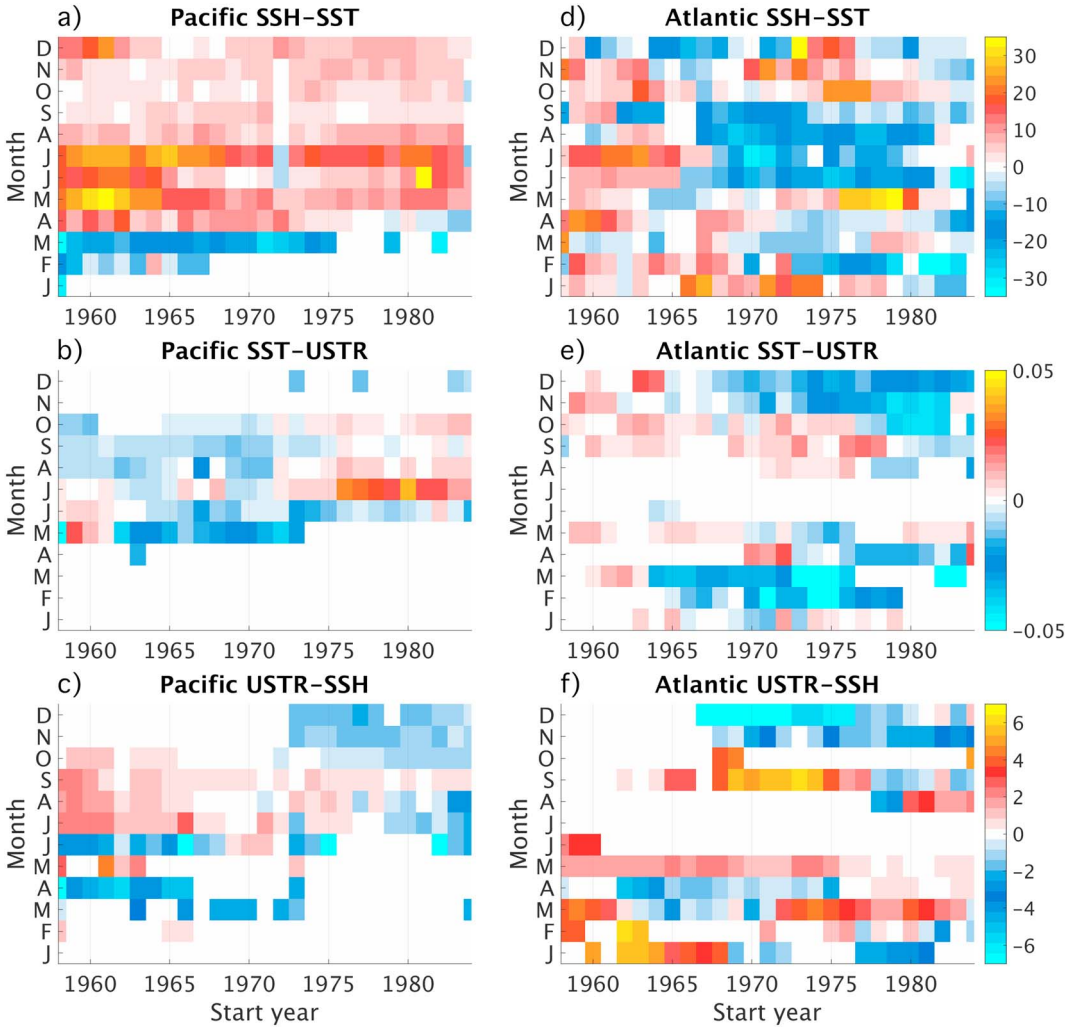

Figure 10. Similar to Figure 9 but showing the difference between positive and negative composites in the Pacific (left column, a–c) and the Atlantic (right column, d–f), for the SSH-SST (a, d), SST-USTR (b, e), and USTR-SSH (c, f) feedback elements. SSH = sea surface height; SST = sea surface temperature; USTR = zonal wind stress.

deviations in the Atlantic (not shown). Because of this and and reasons of consistency, we calculate the composite strengths of our feedback elements in the same manner as above, including a running detrending.

Figures 9 to 11 show the results of our running analysis. The Pacific Bjerknes feedback elements exhibit low-frequency variations (Figure 9). All feedback elements, and generally both the positive and negative composites, show a basic change that occurs around the early 1970s and is characterized by: a weakening subsurface-surface coupling; SST-wind coupling that appears to decrease for the negative composite, but shows no clear change for the positive composite; and strengthening wind-thermocline coupling that is more apparent in the negative composite than in the positive composite. These changes are in rough agreement with the "Pacific climate shift" that took place in 1976/1977 (Ding et al., 2013; Graham, 1994; Trenberth & Hurrell, 1994). A secondary climate shift in the Pacific occurred in 1998/1999, exchanging intense, eastern warm events for a more moderate regime characterized by warm events that occur closer to the center of the basin and are reduced in amplitude (Hu et al., 2012; Lübbecke et al., 2014). Both climate shifts have been related to the low-frequency variability of the Pacific Decadal Oscillation (Minobe, 1997, 2000; Mantua & Hare, 2002, PDO). The 1998/1999 shift, however, is not resolved in our analysis, since our data sets span only 12 years of the postshift era, which constitutes half a period of our running analysis.

As for the OBS-based subsurface-surface coupling discussed in section 3.1, our results for the SSH-SST feedback element are not consistent with Zhu et al. (2015). Seasonalities of the two results disagree (with

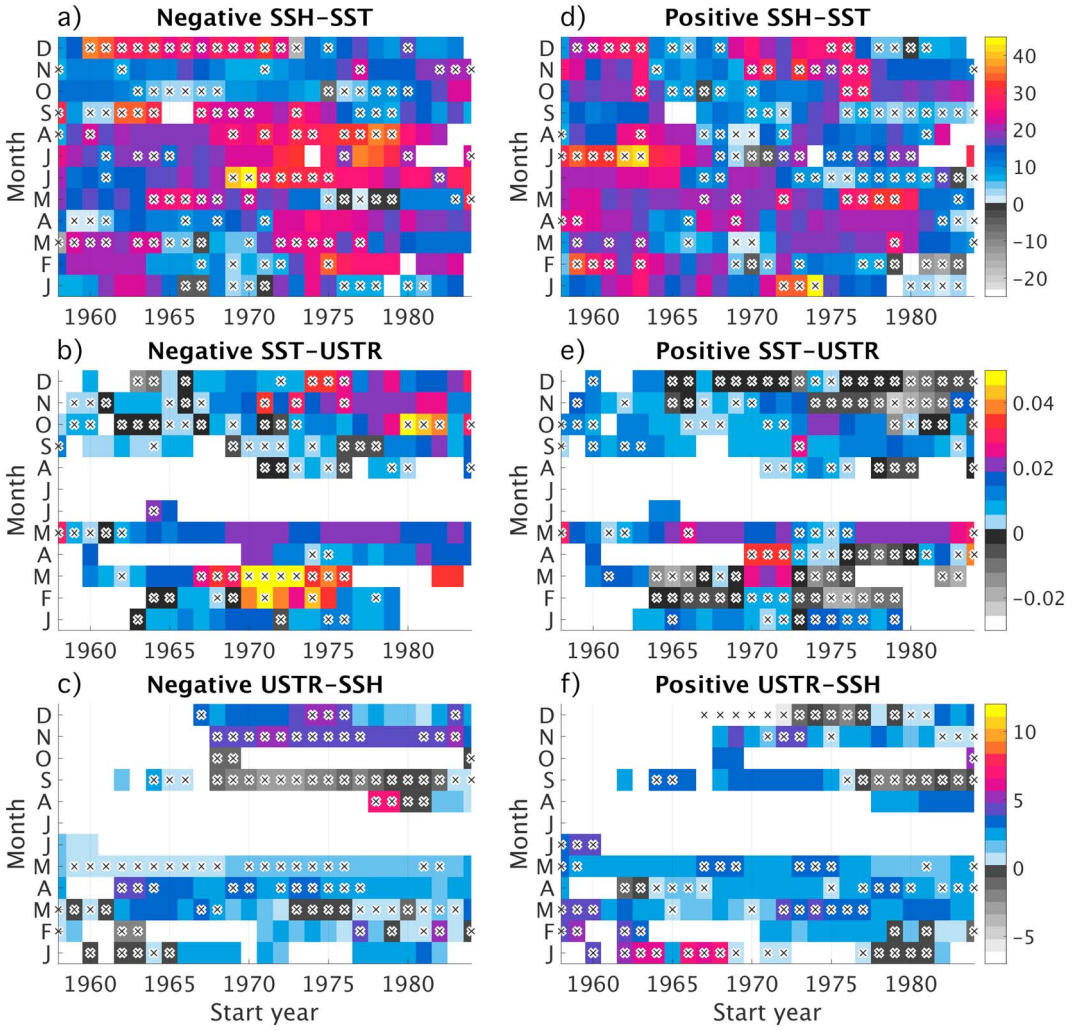

Figure 11. Same as Figure 9 but for the Atlantic. Feedback strengths have been diagnosed with respect to Atl3 for SSH and SST, and with respect to WAtl for USTR. SSH = sea surface height; SST = sea surface temperature; USTR = zonal wind stress.

our SSH-SST feedback elements being strongest in April–June, while Zhu et al.'s (2015) thermocline feedback consistently peaks in September–December). Periods of enhanced subsurface-surface coupling, too, do not agree. In particular, our results indicate that the SSH-SST feedback element was strongest in the period spanning the 1960s to 1990s, for both the positive and the negative composites. Zhu et al. (2015) find fairly consistent thermocline feedbacks in winter, while relationships in boreal spring were very weak in the 1960s–1980s, and again in the mid-1990s to early 2000s. We suspect that methodological differences will most likely explain the apparent discrepancies in seasonality and timing of exceptionally weak or strong relationships: Zhu et al. (2015) used correlations as a measure for the sensitivity between thermocline depth—theirs diagnosed from the depth of the 20 °C-isotherm, ours gleaned from SSH—their running analysis periods had lengths of 11 years in contrast to our 25, and they did not separate positive and negative composites from each other.

While the overall strength composites of the Pacific feedback elements change, the asymmetry between them is largely preserved (Figure 10). An exception is the SST-USTR feedback element (Figure 10b), which displays varying ratios of the positive and negative strength composites.

In the Atlantic, all feedback elements vary substantially on decadal time scales (Figure 11). Even when focusing on the important summer and winter seasons, the symmetries of the Bjerknes feedback elements

change from decade to decade. Subsurface-surface coupling, for example, was the dominant feedback element during the period 1993–2012 (Figures 10d, 11a, and 11d). On decadal time scales, this is not necessarily the case. The SSH-SST feedback element during early boreal summer was dominated by the positive composite in the 1970s and 1980s, and only recently started to draw more strongly from the negative composite. Similarly, the July feedback used to be strongly influenced by the negative composite and only started to be dominated by the positive composite in the mid-1980s. Subsurface-surface coupling in winter, too, has not always been exclusively supported by the negative composite. These shifting symmetries suggest that the relative contributions of positive and negative composites to the SSH-SST feedback element are highly variable on decadal time scales. In a similar fashion, the overall strengths and symmetries of the two wind-related feedback elements changed over the course of the past 50 years.

We conclude that the Atlantic Bjerknes feedback and its symmetry are nonstationary. Keep in mind, however, that the absolute numerical values shown here might be subject to large uncertainties, due to rather short analysis periods and inhomogeneities in the data available to the ORAS4 reanalysis. Hence, while our analysis clearly demonstrates that the Atlantic Bjerknes feedback does vary on decadal time scales, the magnitudes of these variations may not be well constrained by our database.

An important consequence of our findings is that diagnosing the strength of the Atlantic Bjerknes feedback on the basis of a rather long data set might obscure crucial, albeit nonstationary details, in the same manner that averaging over long time scales will effectively lose information on short time scale processes.

5. Summary and Discussion

5.1. Summary

We have studied the symmetry of the Atlantic and Pacific Bjerknes feedbacks, using robust regression to diagnose the strength of the three feedback elements that form the closed Bjerknes feedback loop—the SSH-SST, SST-USTR, and USTR-SSH feedbacks that relate to coupling between the subsurface and surface, SST and wind, and wind and thermocline depth, respectively. Our analysis of the Pacific agrees well with previous research and lends credibility to our results for the Atlantic.

During the recent period 1993–2012 in the Atlantic, asymmetries emerge for all feedback elements during boreal winter and summer, when the Atlantic Bjerknes feedback forms a closed positive feedback loop. During these months, the strengths of all feedback elements are positive, for both types of composites. While both positive and negative composites are strong during boreal summer, the positive composites are much weaker during boreal winter. The two wind-related feedback elements are weaker than their Pacific counterparts and produce summer and winter asymmetries to a varying degree. The total Atlantic Bjerknes feedback is dominated by the negative strength composites in boreal winter and shows mixed influences from positive and negative composites in summer.

Comparing our work with Lübbecke and McPhaden's (2017) study suggested that the results of a feedback analysis in the equatorial Atlantic are highly sensitive to the chosen analysis period. Indeed, our ORAS4-based running analysis of the Atlantic Bjerknes feedback elements provides further evidence for the nonstationarity of the Atlantic Bjerknes feedback. One important result of our study is that conclusions drawn for feedback-related issues in the tropical Atlantic will always have to explicitly consider the analysis period that they are based on.

5.2. Discussion

Taking into account the proposed nonstationarity of the Atlantic Bjerknes feedback, our study serves as a reminder that processes in the coupled equatorial Atlantic climate system can unfold on substantially smaller spatiotemporal scales than their Pacific counterparts. We concede that using even monthly mean data for our analysis might be insufficient to resolve the rapid processes that establish the intricate variability in the tropical Atlantic.

Another problem that we ran into are the very small sample sizes as soon as analysis periods are shorter than 30 years. For our analysis, we used period lengths between 20 and 25 years. Separating the data into positive and negative composites left us with data pools that rarely exceeded the size of 10 to 12 entries per analysis step. To reduce the arbitrariness of our results, we chose robust regression as our analysis method. As our results have demonstrated, decreasing the temporal and spatial extent of our analysis domain reveals important details of the mechanisms that govern the tropical Atlantic.

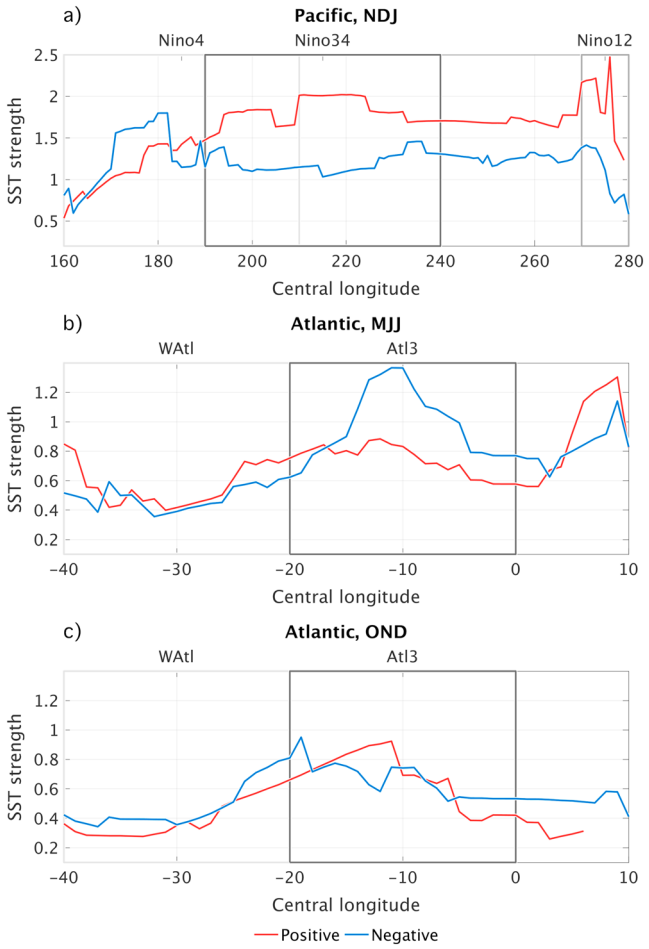

Figure 12. Zonal distribution of the ERSST-based average strength of positive (red) and negative (blue) SST events for the period 1993–2012 (see text for details on how SST events have been diagnosed). SST events have been considered along the equatorial Pacific when they occurred between November and January (NDJ, panel a), and along the equatorial Atlantic when they occurred between May and July (MJJ, b), or between October and December (OND, c). Note that because our analysis period is very short (to match the period for which we diagnosed the lagged, OBS-based feedback element strengths), the number of events diagnosed for each longitude box is smaller than 10. Note also that the *y* axes span different strengths for the Pacific and Atlantic analysis. Overlaid rectangles indicate the Nino4, Nino3.4, and Nino1.2 (WAtl and Atl3) regions in the Pacific (Atlantic). ERSST = extended reconstructed sea surface temperature.

A related issue is that our results concerning the stationarity of the Bjerknes feedback elements rely on a single data set, that is, ORAS4, which in addition is a reanalysis. It would be interesting to assemble additional data sets, preferentially based on direct observations, and repeat our analysis.

To conclude our study, we seek to consolidate the asymmetries that we detected in the recent, OBS-based Pacific and Atlantic Bjerknes feedback with the symmetry of SST variability in the central equatorial ocean basins. Our analysis to this effect is based on SST "events." To identify an SST event, we first calculate the anomalies of the time series with respect to the linear trend and the seasonal cycle. For both positive and negative anomalies separately, we calculate the partial standard deviation. In either case, we select all instances for which anomalies exceed 0.5 times the partial standard deviation. These are potential contributions to events. We next identify periods during which potential contributions have the same sign for at least three consecutive months. These "persisting" anomalies form an SST event. For each event, the anomaly of the largest magnitude provides the strength of the event. We diagnose events in the same 4° longitude × 4° latitude boxes of SST data that we used for our previous analysis.

Figure 12 shows the average strength of positive and negative SST events along the equatorial Pacific and Atlantic, in the same period that we used to diagnose our lagged composite strengths in section 3 (1993–2012). During boreal winter in the Pacific, the well-known amplitude asymmetry emerges (Figure 12a). East of 170°W (190°E), Pacific warm events are substantially stronger than cold events, especially so in the Nino3.4 region. The difference between average warm and cold events can be as high as 1 °C.

In contrast, SST events are much more symmetric in the Atlantic. This agrees with Lübbecke and McPhaden's (2017) findings. Summer Niños during the recent period seem to have been slightly dominated by cold events (Figure 12b), with a maximum difference between negative and positive SST events of about 0.5 °C. This corresponds to the asymmetry of subsurface-surface coupling that we identified in Figure 5a, where the SSH-SST feedback element is clearly stronger for shallow thermoclines (associated with reduced SSTs) than for deep thermoclines (warm SSTs). Considering the total Bjerknes feedback with respect to cold and warm SST conditions softens the relationship (cf. Figures 7d–7f). While the total Bjerknes feedback was indeed stronger when diagnosed with respect to cold SSTs in June, the response to warm SSTs dominated in May and July. (The absolute magnitude of this asymmetry depends on which method is chosen to diagnose the total feedback, cf. section A2 in Appendix A. All methods, however, agree on the negative composite dominating June and the positive composite dominating July. This issue again raises the question whether it is appropriate to weight all feedback elements equally when calculating the total Bjerknes feedback.) Both measures—the strength of subsurface-surface coupling by itself, including lags, and the estimate of the instantaneous total Bjerknes feedback—indicate a weak correspondence between the symmetry of the (total) Bjerknes feedback and the observed, weak amplitude asymmetry.

In contrast, the Atlantic winter Niño is mostly symmetric (Figure 12c), even though the total Bjerknes feedback as well as the SSH-SST and USTR-SSH feedback elements are clearly dominated by their negative composites during boreal winter (Figures 7f, 5d, and 5f). While the (total) Bjerknes feedback is asymmetrical in winter, it does not project onto the observed SST variability—indicating that the Bjerknes feedback plays a minor role in establishing the Atlantic winter Niño. This agrees with Dippe et al. (2018) who have found that dynamical, Bjerknes feedback-related contributions to Atl3 SST variability do increase in winter,

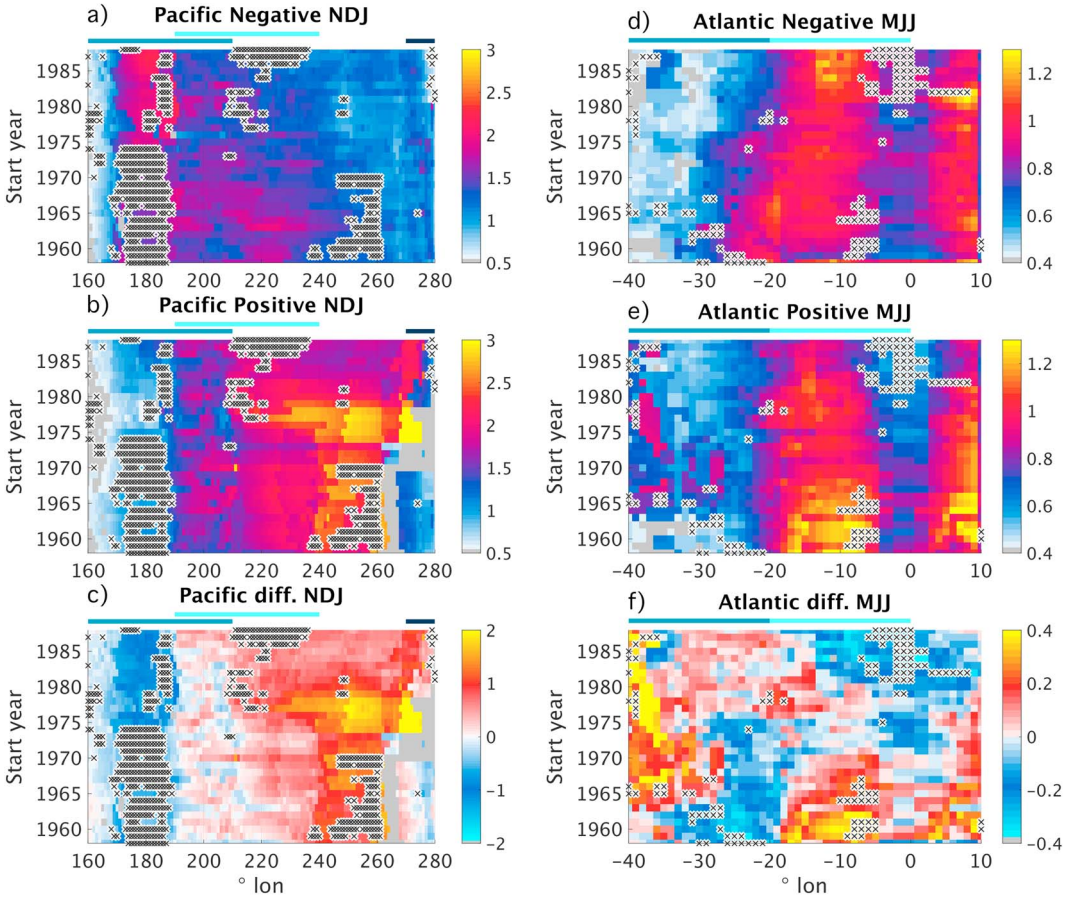

Figure 13. Decadal variations of ERSST-SST event strengths along the equator (*x* axis) for running subperiods (*y* axis, shown dates label the start of each analysis period) in the Pacific (left column, a–c) and the Atlantic (right column, d–f). SST events have only been considered when they peaked in November–January (NDJ) and May–July (MJJ) in the Pacific and Atlantic, respectively. The left, middle, and right columns show the strength of negative and positive SST events, as well as their difference, respectively (see text for details on how SST events have been diagnosed). Black crosses indicate that average negative and positive event strengths are significantly different from each other, according to a Student's *t* test and the significance level 0.1. The length of each subperiod is 25 years, and events have been diagnosed with respect to each subperiod. ERSST = Extended Reconstructed Sea Surface Temperature.

but are much smaller in magnitude than in summer. Rather than being a dynamically driven phenomenon as in the Pacific, the Atlantic winter Niño appears to be much more susceptible to atmospheric noise forcing.

Last, we briefly assess how stationary the symmetry of the Pacific and Atlantic Niños are. Figure 13 shows how the strength of positive and negative SST events varied over the past five decades, using again sliding analysis windows with a length of 25 years each, considering both Pacific events in boreal winter and Atlantic events in boreal summer.

In the Pacific, the basic asymmetry between warm and cold events did not change over the past 50 years (Figures 13a–13c). However, how much warmer the warm events east of 120°W (240°E) are than the corresponding cold events is indeed varying from decade to decade. The strongest asymmetry so far occurred in the 1970s and 1980s, during a warm phase of the Pacific Decadal Oscillation, with average warm events exceeding average cold events by more than 1.5 °C.

In the Atlantic, general characteristics of equatorial SST events have not changed dramatically over the past 50 years, while minor variations do occur (Figures 13d–13f). The location of the strongest cold SST events, for example, appears to have slightly shifted from the western into the central Atl3 region (Figure 13d). Additionally, cold SST events have become stronger within the last 30 years. Warm SST events, on the other hand, have clearly weakened over the past 50 years (Figure 13e), in agreement with Tokinaga and Xie (2011). The resulting effect is that cold events in the eastern equatorial Atlantic dominated the summer Niño during

recent decades, while the 1960s and 1970s seem to have seen stronger warm events (Figure 13f). An interesting detail of this analysis is that asymmetries identified in the Atl3 region do not extend homogeneously toward the eastern edge of the basin. Rather, positive SST events become more pronounced close to the African coast.

These findings complement our results on the decadal modulation of the Bjerknes feedback's strength and could contribute to the understanding of decadal variability in the tropical Pacific and Atlantic. In both ocean basins, a change in the characteristics of the respective Niños has been noted in the 1970s. For the Pacific, this shift has been related to the Pacific Decadal Oscillation (Mantua & Hare, 2002). The 1980s and 1990s were characterized by strong eastern Pacific El Niño events, while the preceding and subsequent decades featured weaker events that occurred more frequently and were more often located in the central equatorial Pacific (An & Wang, 2000; Chung & Li, 2012). In agreement with the 1976/1977 climate shift, all Pacific Bjerknes feedback elements changed in the 1970s (Figures 9a–9c), and the asymmetry between warm and cold events increased correspondingly (Figure 13c).

For the tropical Atlantic, earlier studies on decadal time scales focused mainly on the variability of the interhemispheric SST gradient (Mehta, 1998; Mehta & Delworth, 1995; Wainer et al., 2008), while recent work started to address decadal variations in the eastern equatorial Atlantic SST variability with bearings on the Atlantic Niño. Losada and Rodríguez-Fonseca (2016) describe differences in the spatial pattern of the Atlantic Niño before and after the 1970s, with positive SST anomalies restricted to the eastern equatorial Atlantic in the earlier and a more basin-wide SST signal in the later period. Additionally, Tokinaga and Xie (2011) find a weakening of SST variability in the eastern equatorial Atlantic over the time period 1950 to 2009. These changes are roughly reflected in the weakening of the SSH-SST feedback element's positive composite (Figure 11d) and the associated weakening of the warm events (Figure 13e).

Overall, we have shown that the Atlantic Bjerknes feedback appears to be configured in subtly different ways for positive and negative Atlantic Niño events, both during summer and winter. While these asymmetries project weakly onto the symmetry of summer SST events, the winter Niño is much more susceptible to other influences. Both the Atlantic Bjerknes feedback and the symmetry of the Atlantic Niño appear to vary on decadal time scales.

Appendix A

A1. Using the Same Lags for Positive and Negative Composites

In the main text, we presented composites of the Bjerknes feedback elements and, as discussed in section 2, included feedback lags that we previously diagnosed for our full anomaly time series, disregarding the sign of the forcing variable. Here, we assess whether using these lags enhances our feedback strengths as expected and whether it affects positive and negative composites equally. We do this by repeating our regression analysis, but this time using a constant lag of 0 months for each feedback element ("instantaneous feedback elements"), at all locations and during all months. We then subtract the lagged feedback elements from the instantaneous feedback elements to assess when including lags into our analysis enhances the composite of the feedback element (negative difference). Note that the positive and negative composites that we use are identical in both cases, because they are based on the forcing variable of each feedback element. It is the offset in time of the response variable that differs between the two cases.

Figures A1 and A2 show the difference between the instantaneous and the lagged feedbacks. Including feedback lags into our analysis does enhance the composites of the Bjerknes feedback elements in general. Calculating the mean across all pixels contributing to Figures A1 and A2 yields, both in the Atlantic and the Pacific, negative values for all feedback elements and both composites, except for the positive composite of the Atlantic USTR-SSH feedback element. However, while the overall effect is in agreement with our goals, including the lags can have unexpected local effects.

In the Pacific, including lags into our analysis generally enhances the strength of the feedback composites (Figure A1), with three notable exceptions: First, the negative SSH-SST composite appears to be degraded by lags to the east of the Nino3.4 region for the entire year (Figure A1a). This indicates that subsurface-surface coupling operates in a slightly different manner for negative Pacific Niño events, which in turn is perhaps related to the different average thermocline depths associated with warm and cold Pacific Niños. Second, the negative SST-USTR feedback element composite is degraded by lags during the spring barrier. This,

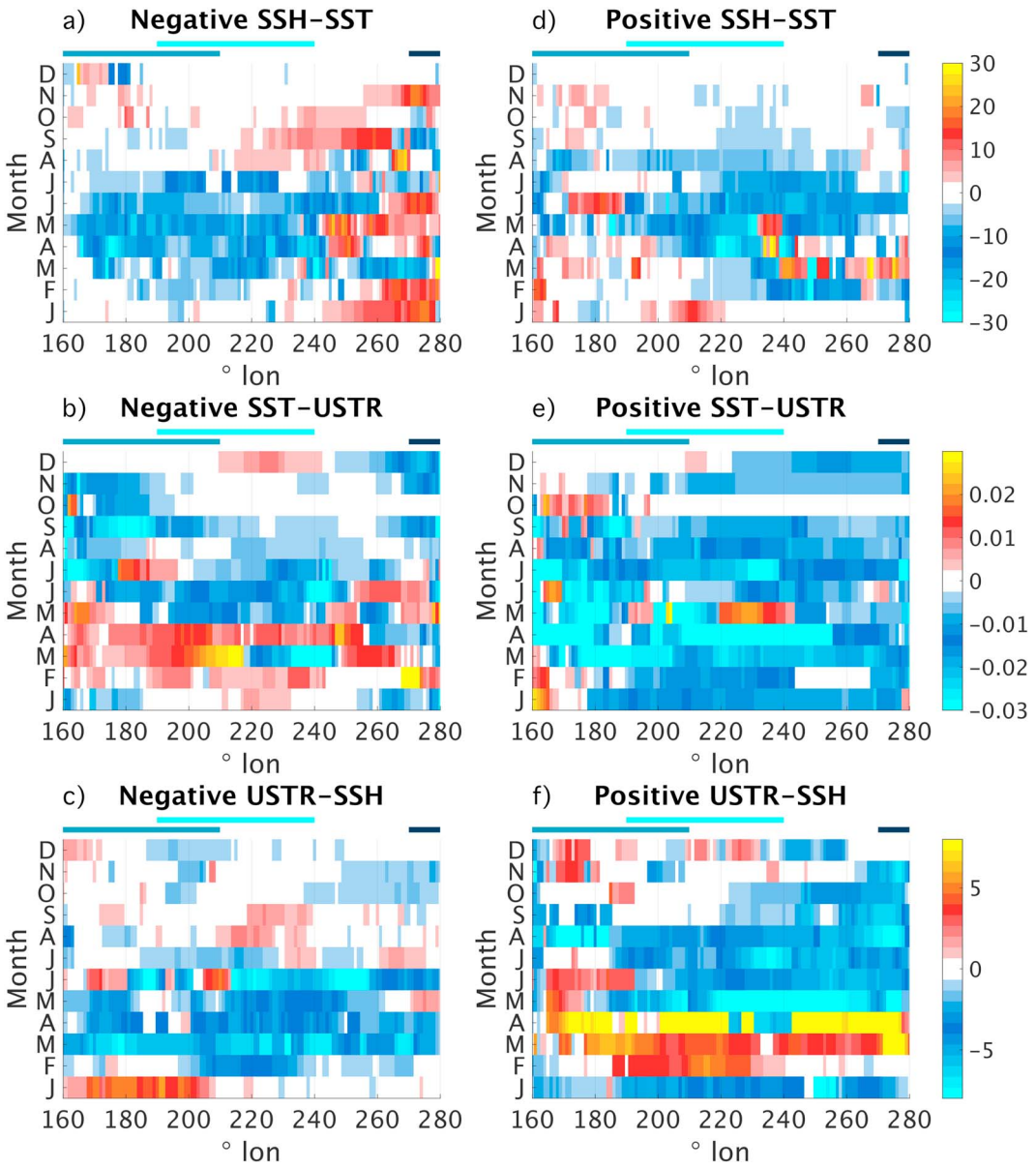

Figure A1. OBS-based comparison between lagged and instantaneous feedback element composites in the Pacific, along the equator (*x* axis) and stratified into calendar months (*y* axis). The instantaneous feedback elements have been diagnosed in the same manner as the lagged feedback elements shown in the main text, but using a constant lag of 0 months when performing robust regression. Positive values indicate that the instantaneous composites are stronger than the lagged composites. Colored bars below the title indicate the zonal extent of the Nino4, Nino3.4, and Nino1.2 regions in blue, light blue, and dark blue, respectively. SSH = sea surface height; SST = sea surface temperature; USTR = zonal wind stress.

however, is of no practical concern, since the overall coupling during boreal spring in any case is decreased. Third, in a similar fashion, the positive USTR-SSH feedback element during the spring barrier clearly suffers when incorporating lags.

Figure A2 shows that the impact of lags on Atlantic feedback strengths is less straightforward than that in the Pacific. While lags generally enhance the feedback strengths, they can have severely detrimental effects in certain regions and seasons. Three notable cases are as follows: First, similar to the Pacific, the lags of the SSH-SST feedback element differ from each other; unlike in the Pacific, they do so during the crucial month of May (Figures 2a and 2d of the main text). Here, lags strongly decrease the positive composite of the SSH-SST feedback element. The overall effect of this degradation, however, is small, since the corresponding

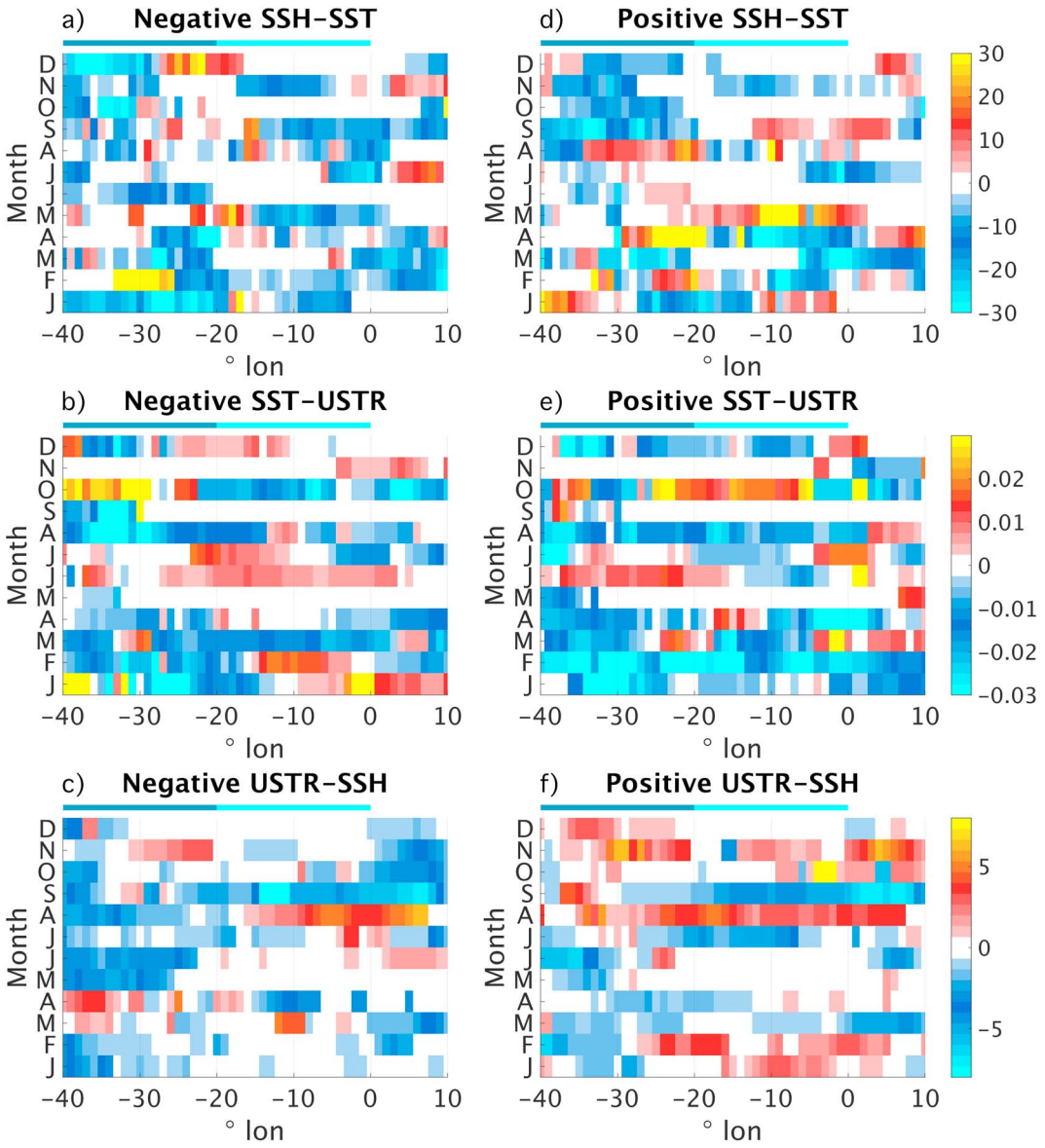

Figure A2. Same as Figure A1 but for the Atlantic. Overlaid colored rectangles indicate the zonal extent of the WAtl and Atl3 regions. SSH = sea surface height; SST = sea surface temperature; USTR = zonal wind stress.

lagged negative composite is clearly enhanced by the incorporation of lags. The overall May asymmetry between the positive and negative composites of the SSH-SST feedback element remains intact. Second, the negative SST-USTR feedback element composite suffers when using lags in June and July (Figure A2b). These months, however, are characterized by weakly negative lags (Figure 2e of the main text) and we expect that they do not contribute substantially to the closed Atlantic Bjerknes feedback. Third, in a similar fashion, the August degradations of both the positive and the negative USTR-SSH feedback element composites are of no practical concern.

Overall, we conclude that using a constant lag for positive and negative feedback element strength composites does, in general, enhance the strength of the feedbacks as expected. When exceptions occur, they are usually related to negative lags that are of little importance for the closed Bjerknes feedback.

Nevertheless, this simple comparison serves to demonstrate again how diverse the mechanisms are that produce the variability of the Atlantic and Pacific Niños and that it may not be justified to make equivalent assumptions for warm and cold events.

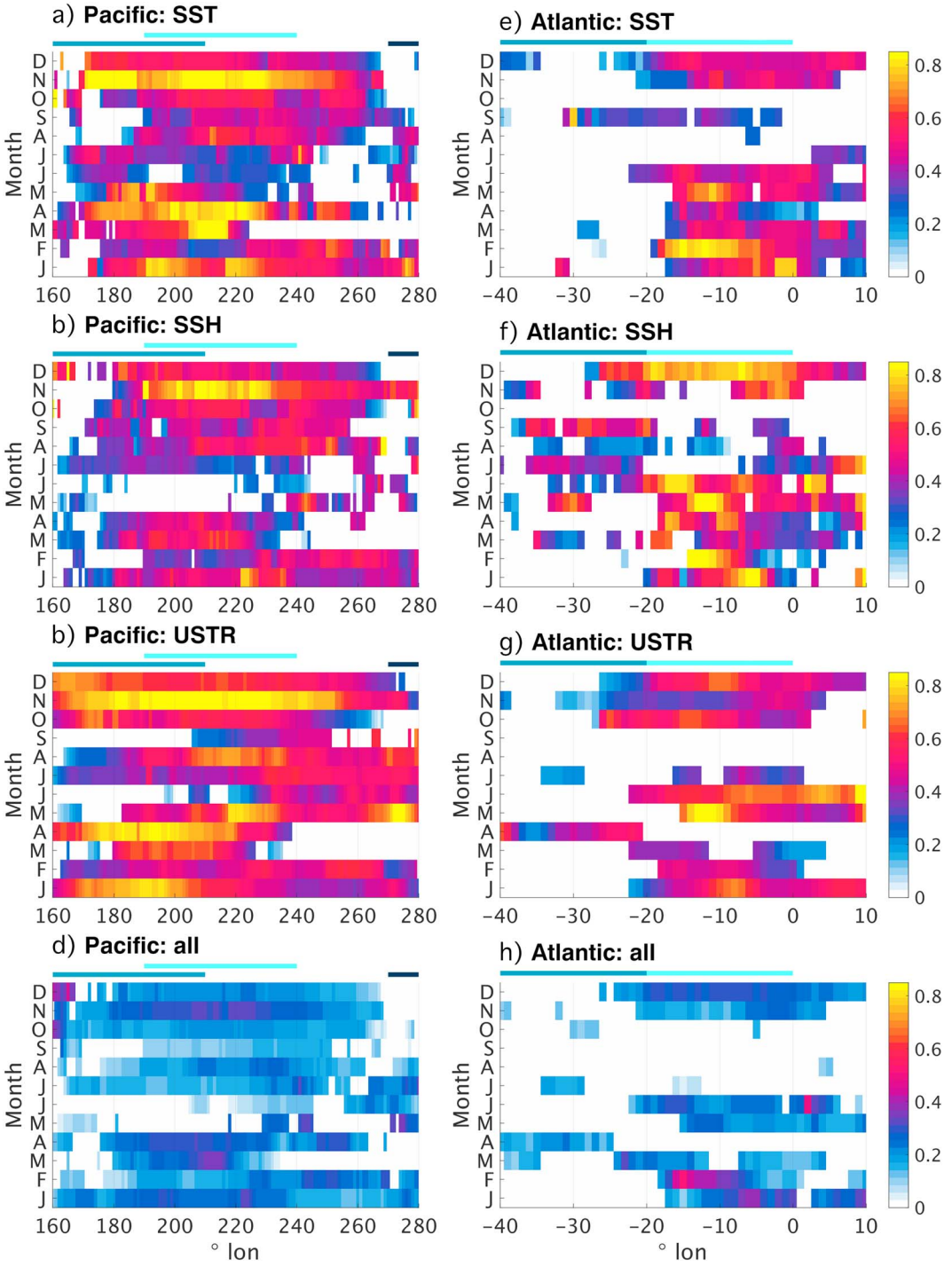

Figure A3. OBS-based comparison of different manifestations of the negative composite of the total Bjerknes feedback in the Pacific (left column, a–d) and the Atlantic (right column, e–h) for the period 1993–2012. All panels show total feedbacks along the equator (*x* axis) and stratified into calendar months (*y* axis). The first, second, third, and fourth rows show the negative composites of the total Bjerknes feedback using constant composites based on SST (a, e; these are the same as in the main text), SSH (b, f), and USTR (c, g), and variable composites (d, h; see text for details on the differences between the manifestations). Recall that the SST/SSH/USTR-based total feedback composites are a measure of the total Bjerknes feedback for when the SST/thermocline/zonal wind stress in the western ocean basin is warmer/deeper/more easterly (positive anomalies) or cooler/shallower/more westerly (negative anomalies) than on average. White indicates that at least one of the feedback elements contributing to the composite of the total feedback was negative. Colored bars below the title indicate the zonal extent of the Nino4, Nino3.4, and Nino1.2 (WAtl and ATl3) regions in blue, light blue, and dark blue (blue and light blue) in the Pacific (Atlantic), respectively. SSH = sea surface height; SST = sea surface temperature; USTR = zonal wind stress.

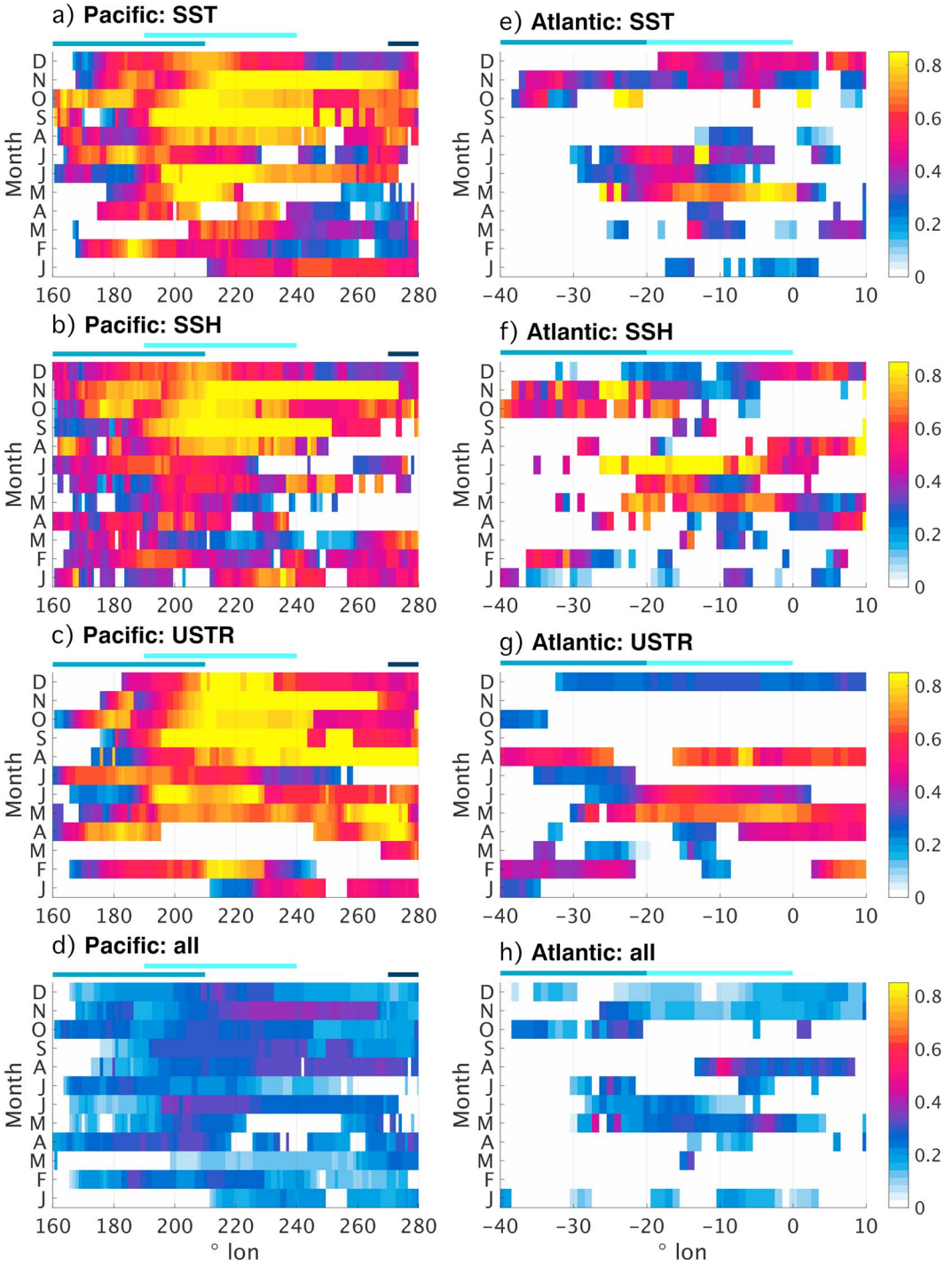

Figure A4. Same as Figure A3 but for manifestations of the positive composites of the total Bjerknes feedback.

A2. On the Sensitivity of the Total Feedback to Different Diagnosis Methods

In addition to the SST-based total feedback shown in the main text, we present three ancillary manifestations of the total Bjerknes feedback in Figures A3–A5.

We diagnose the total Bjerknes feedback in two ways, depending on which subset of our data we select to calculate the strength of the three feedback elements contributing to the total feedback composites.

1. *Constant-composite* total feedbacks (panels a, b, d, and e in Figures A3 to A5): Composites of the individual Bjerknes feedback are identical. This is the method that was used to diagnose the SST-based total feedback

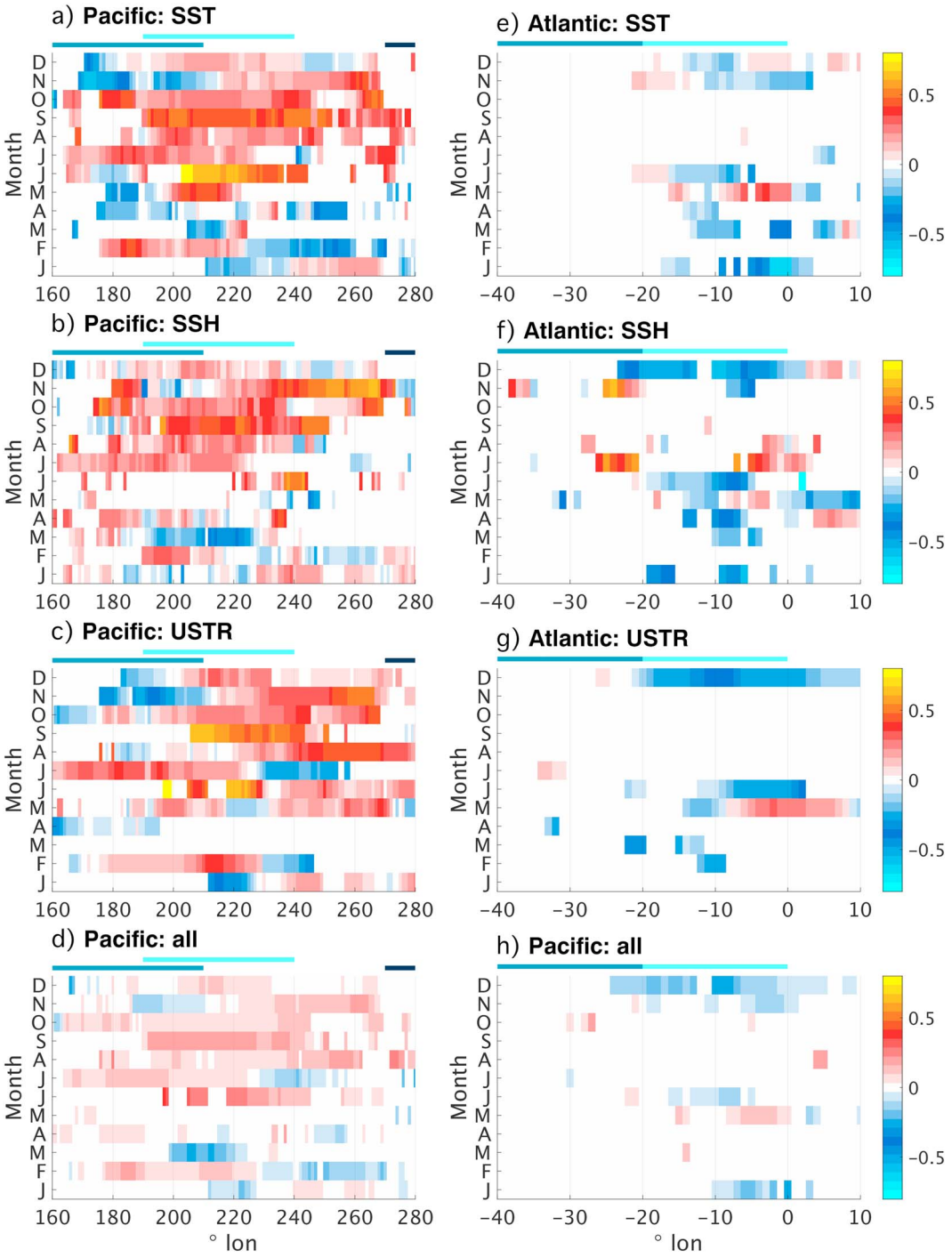

Figure A5. Same as Figure A3, but for the difference between the positive and negative composites of different manifestations of the total Bjerknes feedback.

shown in the main text. Total feedbacks of this class are directly linked to a single variable. The SST-based total feedbacks are a measure of the strength of the total feedback *when SST anomalies are either positive or negative*. Likewise, negative/positive USTR-based and SSH-based total feedback composites are associated with westerly/easterly wind stress anomalies and shallower/deeper thermocline depths, respectively.

2. *Variable-composite* total feedbacks (panels c and f in Figures A3 to A5): For each feedback element, we use individual, "native" composites that depend on the specific feedback element. This method is congruent with the way we diagnosed our lagged feedback elements in section 3.1 of the main text. Composites for

the SSH-SST, SST-USTR, and USTR-SSH feedback elements are based on the sign of SSH, SST, and USTR anomalies, respectively. Again, this means that positive composites of any two feedback elements do not necessarily share the same base data.

In the Pacific, results are consistent between different manifestations of the total Bjerknes feedback (panels a–c of Figures A3 to A5). Seasonalities of positive and negative total feedback composites are well comparable for all manifestations, as are the relative strengths. This highlights the large-scale character of the Pacific Niño, showing that SSH, SST, and USTR vary largely synchronously when measured at the same calendar months during periods when the total Bjerknes feedback is strong. On the other hand, constant-composite feedbacks can be twice as strong as the corresponding variable-composite feedbacks, according to our simple measure. This perhaps indicates that using constant composites prevents compensation effects between the three individual feedback elements. Providing consistent composites for all feedback elements in the constant-composite case emphasizes interactions between all three variables, while the variable-composite case focuses on interactions of only two variables, ignoring the third link in the Bjerknes feedback loop.

In the Atlantic, results are largely consistent for different manifestations of the total Bjerknes feedback (panels d–f of Figures A3–A5). Irrespective of the compositing type, total feedbacks are stronger when they are associated with negative anomalies in boreal winter, and weaker in summer. As in the Pacific, details differ between the three constant-composite manifestations, and the variable-composite manifestation produces weaker total feedbacks. A prominent example are the positive composites of the constant-composite manifestations in July. For this calendar month, the total feedback is pronounced for deep thermoclines, moderately strong for warm SSTs, and effectively absent for easterly wind stress anomalies. However, as our base data pool only spans 20 years in total and we subdivide these further into positive and negative composites, we expect that the details of our analysis are subject to large uncertainties.

Overall, qualitative results are consistent when comparing different manifestations of the total Bjerknes feedback, lending credibility to our method. While details differ for the three constant-composite feedbacks, results are much more sensitive to the choice of either constant or variable composites when diagnosing the individual feedback elements contributing to the total feedback.

Acknowledgments
This study has been supported by the German Ministry for Education and Research (BMBF) through MiKlip2, subproject 01LP1517D (ATMOS-MODINI) and SACUS (03G0837A), and by the European Union 7th Framework Programme (FP7 2007–2013) under grant agreement 603521 PREFACE project. R. J. G. is also grateful for continuing support from GEOMAR. The Matlab scripts that have been used to carry out the analyses for this study have been published and are available online (DOI: 10.3289/sw_1_2019) via GEOMAR's Git and OceanRep.

References

An, S.-I., & Wang, B. (2000). Interdecadal change of the structure of the ENSO mode and its impact on the ENSO frequency. *Journal of Climate*, *13*(12), 2044–2055. https://doi.org/10.1175/1520-0442(2000)013h2044:ICOTSOi2.0.CO;2

Ashok, K., & Yamagata, T. (2009). The El Niño with a difference. *Nature*, *461*, 481–484. https://doi.org/10.1038/461481a

Balmaseda, M. A., Mogensen, K., & Weaver, A. T. (2012). Evaluation of the ECMWF ocean reanalysis system ORAS4. *Quarterly Journal of the Royal Meteorological Society*, *139*(674), 1132–1161. https://doi.org/10.1002/qj.2063

Bjerknes, J. (1966). A possible response of the atmospheric Hadley circulation to equatorial anomalies of ocean temperature. *Tellus*, *18*(4), 820–829. https://doi.org/10.3402/tellusa.v18i4.9712

Bjerknes, J. (1969). Atmospheric teleconnections from the equatorial Pacific. *Monthly Weather Review*, *97*(3), 163–172. https://doi.org/10.1175/1520-0493(1969)097h0163:ATFTEPi2.3.CO;2

Burls, N. J., Reason, C. J. C., Penven, P., & Philander, S. G. (2011). Similarities between the tropical Atlantic seasonal cycle and ENSO: An energetics perspective. *Journal of Geophysical Research*, *116*, C11010. https://doi.org/10.1029/2011JC007164

Burls, N. J., Reason, C. J. C., Penven, P., & Philander, S. G. (2012). Energetics of the tropical Atlantic zonal mode. *Journal of Climate*, *25*(21), 7442–7466. https://doi.org/10.1175/JCLI-D-11-00602.1

Cane, M. A. (1984). Modeling sea level during El Niño. *Journal of Physical Oceanography*, *14*(12), 1864–1874. https://doi.org/10.1175/1520-0485(1984)014h1864:MSLDENi2.0.CO;2

Capotondi, A., Wittenberg, A. T., Newman, M., Di Lorenzo, E., Yu, J.-Y., Braconnot, P., et al. (2015). Understanding ENSO diversity. *Bulletin of the American Meteorological Society*, *96*(6), 921–938. https://doi.org/10.1175/BAMS-D-13-00117.1

Chen, D., Lian, T., Fu, C., Cane, M. A., Tang, Y., Murtugudde, R., et al. (2015). Strong influence of westerly wind bursts on El Nino diversity. *Nature Geoscience*, *8*(5), 339–345. https://doi.org/10.1038/ngeo2399

Chung, P.-H., & Li, T. (2012). Interdecadal relationship between the mean state and El Niño types. *Journal of Climate*, *26*(2), 361–379. https://doi.org/10.1175/JCLI-D-12-00106.1

Cobb, K. M., Westphal, N., Sayani, H. R., Watson, J. T., Di Lorenzo, E., Cheng, H., et al. (2013). Highly variable El Niño-Southern Oscillation throughout the Holocene. *Science*, *339*(6115), 67 LP–70. http://science.sciencemag.org/content/339/6115/67.abstract

Dee, D. P., Uppala, S. M., Simmons, A. J., Berrisford, P., Poli, P., Kobayashi, S., et al. (2011). The ERA-Interim reanalysis: Configuration and performance of the data assimilation system. *Quarterly Journal of the Royal Meteorological Society*, *137*(656), 553–597. https://doi.org/10.1002/qj.828

Delworth, T. L., & Mann, M. E. (2000). Observed and simulated multidecadal variability in the Northern Hemisphere. *Climate Dynamics*, *16*(9), 661–676. https://doi.org/10.1007/s003820000075

Deppenmeier, A.-L., Haarsma, R. J., & Hazeleger, W. (2016). The Bjerknes feedback in the tropical Atlantic in CMIP5 models. *Climate Dynamics*, *47*, 1–17. https://doi.org/10.1007/s00382-016-2992-z

DiNezio, P. N., & Deser, C. (2014). Nonlinear controls on the persistence of La Niña. *Journal of Climate*, *27*(19), 7335–7355. https://doi.org/10.1175/JCLI-D-14-00033.1

Ding, H., Greatbatch, R. J., Latif, M., Park, W., & Gerdes, R. (2013). Hindcast of the 1976/77 and 1998/99 climate shifts in the Pacific. *Journal of Climate*, *26*(19), 7650–7661. https://doi.org/10.1175/JCLI-D-12-00626.1

Dippe, T., Greatbatch, R. J., & Ding, H. (2018). On the relationship between Atlantic Niño variability and ocean dynamics. *Climate Dynamics*, *51*(1), 597–612. https://doi.org/10.1007/s00382-017-3943-z

Dommenget, D., Bayr, T., & Frauen, C. (2013). Analysis of the non-linearity in the pattern and time evolution of El Niño Southern Oscillation. *Climate Dynamics*, *40*(11), 2825–2847. https://doi.org/10.1007/s00382-012-1475-0

Duan, W., & Wei, C. (2013). The 'spring predictability barrier' for ENSO predictions and its possible mechanism: Results from a fully coupled model. *International Journal of Climatology*, *33*(5), 1280–1292. https://doi.org/10.1002/joc.3513

Gill, A. E. (1980). Some simple solutions for heat-induced tropical circulation. *Quarterly Journal of the Royal Meteorological Society*, *106*(449), 447–462. https://doi.org/10.1002/qj.49710644905

Graham, N. E. (1994). Decadal-scale climate variability in the tropical and North Pacific during the 1970s and 1980s: Observations and model results. *Climate Dynamics*, *10*(3), 135–162. https://doi.org/10.1007/BF00210626

Holland, P. W., & Welsch, R. E. (1977). Robust regression using iteratively reweighted least-squares. *Communications in Statistics - Theory and Methods*, *6*(9), 813–827. https://doi.org/10.1080/03610927708827533

Hu, Z.-Z., Kumar, A., Huang, B., Zhu, J., Zhang, R.-H., & Jin, F.-F. (2017). Asymmetric evolution of El Niño and La Niña: The recharge/discharge processes and role of the off-equatorial sea surface height anomaly. *Climate Dynamics*, *49*(7), 2737–2748. https://doi.org/10.1007/s00382-016-3498-4

Hu, Z.-Z., Kumar, A., Ren, H.-L., Wang, H., L'Heureux, M., & Jin, F.-F. (2012). Weakened interannual variability in the tropical Pacific Ocean since 2000. *Journal of Climate*, *26*(8), 2601–2613. https://doi.org/10.1175/JCLI-D-12-00265.1

Huang, B., Thorne, P. W., Banzon, V. F., Boyer, T., Chepurin, G., Lawrimore, J. H., et al. (2017). Extended reconstructed sea surface temperature, Version 5 (ERSSTv5): Upgrades, validations, and intercomparisons. *Journal of Climate*, *30*(20), 8179–8205. https://doi.org/10.1175/JCLI-D-16-0836.1

Huber, P. J., & Ronchetti, E. M. (2009). *Robust statistics* (2nd ed.). Hoboken, N.J: Wiley.

Hummels, R., Dengler, M., & Bourlès, B. (2013). Seasonal and regional variability of upper ocean diapycnal heat flux in the Atlantic cold tongue. *Progress in Oceanography*, *111*, 52–74. https://doi.org/10.1016/j.pocean.2012.11.001

Jin, F. F., Kim, S. T., & Bejarano, L. (2006). A coupled-stability index for ENSO. *Geophysical Research Letters*, *33*, L23708. https://doi.org/10.1029/2006GL027221

Keenlyside, N. S., & Latif, M. (2007). Understanding equatorial Atlantic interannual variability. *Journal of Climate*, *20*(1), 131–142. https://doi.org/10.1175/JCLI3992.1

Knight, J. R., Folland, C. K., & Scaife, A. A. (2006). Climate impacts of the Atlantic multidecadal oscillation. *Geophysical Research Letters*, *33*, L17706. https://doi.org/10.1029/2006GL026242

Levine, A. F. Z., & Jin, F. F. (2017). A simple approach to quantifying the noise-ENSO interaction. Part I: Deducing the state-dependency of the windstress forcing using monthly mean data. *Climate Dynamics*, *48*(1), 1–18. https://doi.org/10.1007/s00382-015-2748-1

Levine, A. F. Z., & McPhaden, M. J. (2016). How the July 2014 easterly wind burst gave the 2015–2016 El Niño a head start. *Geophysical Research Letters*, *43*, 6503–6510. https://doi.org/10.1002/2016GL069204

Li, J., Xie, S.-P., Cook, E. R., Morales, M. S., Christie, D. A., Johnson, N. C., et al. (2013). El Niño modulations over the past seven centuries. *Nature Climate Change*, *3*, 822.

Losada, T., & Rodríguez-Fonseca, B. (2016). Tropical atmospheric response to decadal changes in the Atlantic equatorial mode. *Climate Dynamics*, *47*(3-4), 1211–1224. https://doi.org/10.1007/s00382-015-2897-2

Lübbecke, J. F., Burls, N. J., Reason, C. J. C., & McPhaden, M. J. (2014). Variability in the south Atlantic anticyclone and the Atlantic Niño mode. *Journal of Climate*, *27*(21), 8135–8150. https://doi.org/10.1175/JCLI-D-14-00202.1

Lübbecke, J. F., & McPhaden, M. J. (2013). A comparative stability analysis of Atlantic and Pacific Niño modes. *Journal of Climate*, *26*(16), 5965–5980. https://doi.org/10.1175/JCLI-D-12-00758.1

Lübbecke, J. F., & McPhaden, M. J. (2017). Symmetry of the Atlantic Niño mode. *Geophysical Research Letters*, *44*, 965–973. https://doi.org/10.1002/2016GL071829

Mantua, N. J., & Hare, S. R. (2002). The Pacific decadal oscillation. *Journal of Oceanography*, *58*(1), 35–44. https://doi.org/10.1023/A:1015820616384

Martín-Rey, M., Polo, I., Rodríguez-Fonseca, B., Losada, T., & Lazar, A. (2017). Is there evidence of changes in tropical Atlantic variability modes under AMO phases in the observational record?. *Journal of Climate*, *31*(2), 515–536. https://doi.org/10.1175/JCLI-D-16-0459.1

Mehta, V. M. (1998). Variability of the tropical ocean surface temperatures at decadal-multidecadal timescales. Part I: The Atlantic Ocean. *Journal of Climate*, *11*(9), 2351–2375. https://doi.org/10.1175/1520-0442(1998)011%3C2351:VOTTOS%3E2.0.CO

Mehta, V. M., & Delworth, T. (1995). Decadal variability of the tropical Atlantic Ocean surface temperature in shipboard measurements and in a global ocean-atmosphere model. *Journal of Climate*, *8*(2), 172–190. https://doi.org/10.1175/1520-0442(1995)008h0172:DVOTTAi2.0.CO;2

Minobe, S. (1997). A 50-70 year climatic oscillation over the North Pacific and North America. *Geophysical Research Letters*, *24*(6), 683–686. https://doi.org/10.1029/97GL00504

Minobe, S. (2000). Spatio-temporal structure of the pentadecadal variability over the North Pacific. *Progress in Oceanography*, *47*(2), 381–408. https://doi.org/10.1016/S0079-6611(00)00042-2

Okumura, Y., & Xie, S. P. (2006). Some overlooked features of tropical Atlantic climate leading to a new Niño-like phenomenon. *Journal of Climate*, *19*(22), 5859–5874.

Rebert, J. P., Donguy, J. R., Eldin, G., & Wyrtki, K. (1985). Relations between sea level, thermocline depth, heat content, and dynamic height in the tropical Pacific Ocean. *Journal of Geophysical Research*, *90*(C6), 11,719–11,725. https://doi.org/10.1029/JC090iC06p11719

Richter, I., Behera, S. K., Masumoto, Y., Taguchi, B., Sasaki, H., & Yamagata, T. (2013). Multiple causes of interannual sea surface temperature variability in the equatorial Atlantic Ocean. *Nature Geoscience*, *6*(1), 43–47. https://doi.org/10.1038/ngeo1660

Schlesinger, M. E., & Ramankutty, N. (1994). An oscillation in the global climate system of period 65-70 years. *Nature*, *367*, 723. https://doi.org/10.1038/367723a0

Smith, T. M., & Reynolds, R. W. (2003). Extended reconstruction of global sea surface temperatures based on COADS data (1854-1997). *Journal of Climate*, *16*(10), 1495–1510. https://doi.org/10.1175/1520-0442-16.10.1495

Street, J. O., Carroll, R. J., & Ruppert, D. (1988). A note on computing robust regression estimates via iteratively reweighted least squares. *The American Statistician*, *42*(2), 152–154. https://doi.org/10.1080/00031305.1988.10475548

Takahashi, K., & Dewitte, B. (2016). Strong and moderate nonlinear El Niño regimes. *Climate Dynamics*, *46*(5), 1627–1645. https://doi.org/10.1007/s00382-015-2665-3

Takahashi, K., Montecinos, A., Goubanova, K., & Dewitte, B. (2011). ENSO regimes: Reinterpreting the canonical and Modoki El Niño. *Geophysical Research Letters*, *38*, L10704. https://doi.org/10.1029/2011GL047364

Timmermann, A., An, S.-I., Kug, J.-S., Jin, F.-F., Cai, W., Capotondi, A., et al. (2018). El Niño-Southern Oscillation complexity. *Nature*, *559*(7715), 535–545. https://doi.org/10.1038/s41586-018-0252-6

Tokinaga, H., & Xie, S.-P. (2011). Weakening of the equatorial Atlantic cold tongue over the past six decades. *Nature Geoscience*, *4*(4), 222–226. https://doi.org/10.1038/ngeo1078

Torrence, C., & Webster, P. J. (1998). The annual cycle of persistence in the El Nño/Southern Oscillation. *Quarterly Journal of the Royal Meteorological Society*, *124*(550), 1985–2004. https://doi.org/10.1002/qj.49712455010

Trenberth, K. E., & Hurrell, J. W. (1994). Decadal atmosphere-ocean variations in the Pacific. *Climate Dynamics*, *9*(6), 303–319. https://doi.org/10.1007/BF00204745

Uppala, S. M., Kållberg, W. P., Simmons, J. A., Andrae, U., Costa, B., Fiorino, M., et al. (2006). The ERA-40 re-analysis. *Quarterly Journal of the Royal Meteorological Society*, *131*(612), 2961–3012. https://doi.org/10.1256/qj.04.176

Wainer, I., Servain, J., & Clauzet, G. (2008). Is the decadal variability in the tropical Atlantic a precursor to the NAO? *Annales Geophysicae: Atmospheres, Hydrospheres and Space Sciences*, *26*(12), 4075.

Wengel, C., Latif, M., Park, W., Harlaß, J., & Bayr, T. (2018). Seasonal ENSO phase locking in the Kiel climate model: The importance of the equatorial cold sea surface temperature bias. *Climate Dynamics*, *50*, 901–919. https://doi.org/10.1007/s00382-017-3648-3

Xie, S.-P., Tanimoto, Y., Noguchi, H., & Matsuno, T. (1999). How and why climate variability differs between the tropical Atlantic and Pacific. *Geophysical Research Letters*, *26*(11), 1609–1612. https://doi.org/10.1029/1999GL900308

Yeh, S.-w., Kug, J.-s., Dewitte, B., Kwon, M.-h., Kirtman, B. P., & Jin, F.-f. (2009). El Niño in a changing climate. *Nature*, *461*(7263), 511–4. https://doi.org/10.1038/nature08316

Zebiak, S. E., & Cane, M. A. (1987). A model El Niño-Southern Oscillation. *Monthly Weather Review*, *115*(10), 2262–2278. https://doi.org/10.1175/1520-0493(1987)115h2262:AMENOi2.0.CO;2

Zheng, F., Fang, X.-H., Yu, J.-Y., & Zhu, J. (2014). Asymmetry of the Bjerknes positive feedback between the two types of El Niño. *Geophysical Research Letters*, *41*, 7651–7657. https://doi.org/10.1002/2014GL062125

Zhu, J., Kumar, A., & Huang, B. (2015). The relationship between thermocline depth and SST anomalies in the eastern equatorial Pacific: Seasonality and decadal variations. *Geophysical Research Letters*, *42*, 4507–4515. https://doi.org/10.1002/2015GL064220